Article

Discovery Medicine 2026; 38(206): 936–958
https://doi.org/10.24976/Discov.Med.202638206.76

CPAMD8 and *EGR1* are Potential Prognostic Signature Genes Associated With Olaparib and Niraparib Resistance in Ovarian Cancer

Dan Zhou[1,2], Sijia Cheng[2,3,4], Jiayi Li[4,5], Tianle Mao[2,6], Jiaru Luo[4], Minghui Zhou[2], Tingting Luo[4], Jinlin Du[5], Yunzhi Ling[4,*], Yanqin Ji[2,*]

[1]The First School of Clinical Medicine, Jinan University, 510632 Guangzhou, Guangdong, China
[2]Department of Gynecology, Huizhou Central People's Hospital, 516001 Huizhou, Guangdong, China
[3]Laboratory of Human Virology and Oncology, Shantou University Medical College, 515041 Shantou, Guangdong, China
[4]Science Research Center, Huizhou Central People's Hospital, 516001 Huizhou, Guangdong, China
[5]Department of Epidemiology and Statistics, School of Public Health, Guangdong Medical University, 523808 Dongguan, Guangdong, China
[6]The First School of Clinical Medicine, Guangdong Medical University, 524023 Zhanjiang, Guangdong, China
*Correspondence: lyz@algaemedical.com (Yunzhi Ling); yanqinjihzch@163.com (Yanqin Ji)
Submitted: 15 December 2025 Revised: 12 February 2026 Accepted: 27 February 2026 Published: 20 March 2026

Background: Poly(ADP-ribose) polymerase inhibitors (PARPis) are effective adjunctive therapies for ovarian cancer (OC). However, drug resistance remains a significant clinical challenge. Current research focuses on target expression and functional changes in established resistant cell lines. Yet, a comprehensive analysis of transcriptomic alterations over time after PARPis exposure is lacking. This study aims to investigate the transcriptomic changes in OC cell lines following prolonged PARPis treatment and to identify potential resistance biomarkers.

Methods: SKOV3 and OVCAR8 cell lines were treated with Olaparib and Niraparib for 2, 3 and 6 months, and then RNA sequencing (RNA-seq) was performed. Differentially expressed genes (DEGs) were identified through "limma" analysis, following the conduction of function enrichment analysis. Survival analysis was performed using The Cancer Genome Atlas (TCGA) data to correlate DEG expression with clinical outcomes. To validate the identified key resistance genes, we modulated their expression using specific siRNAs for knockdown and overexpression vectors. We performed these experiments in ovarian cancer cells following long-term culture with PARPis. Models included SKOV3 and OVCAR8 cells, which were maintained for 6 months with either Niraparib (SKOV3_Nira_6M, OVCAR8_Nira_6M) or Olaparib (SKOV3_Ola_6M, OVCAR8_Ola_6M). We then assessed proliferation and viability to confirm the functional relevance of these genes to PARPis sensitivity in ovarian cancer.

Results: The transcriptional profiles of the same type of OC cells stimulated by Niraparib and Olaparib for 6 months were highly similar. After SKOV3 cells were treated with PARPis for 6 months, 59 DEGs showed consistent changes, while 103 DEGs were identified in OVCAR8 cells (adjusted $p < 0.05$ and $|\log_2 \text{fold change}| > 1$). These DEGs were enriched in biological processes such as epithelial cell differentiation ($p < 0.05$), estrogen receptor signaling ($p < 0.05$), and cell adhesion ($p < 0.05$), among others. Among them, we found that *CPAMD8* ($p < 0.05$) and *EGR1* were specifically upregulated in SKOV3 (adjusted $p < 0.05$) and OVCAR8 (adjusted $p < 0.05$) cells after 6 months of PARPis stimulation, and they were significantly associated with poor overall survival in OC patients. Further validation in vitro confirmed that both mRNA and protein levels of *CPAMD8* and *EGR1* were significantly elevated in SKOV3 and OVCAR8 cells following 6 months of maintenance culture with PARPis. Building on these findings, functional studies demonstrated that enforced overexpression of *CPAMD8* or *EGR1* in these PARPis-persistent cells markedly enhanced cell viability. In contrast, knockdown of *CPAMD8* or *EGR1* expression effectively suppressed cell viability.

Conclusion: *CPAMD8* and *EGR1* were identified as potential biomarkers of mild drug resistance and were associated with poorer survival.

Keywords: ovarian cancer; Olaparib; Niraparib; poly(ADP-ribose) polymerase inhibitor resistance; RNA sequencing; C3 and PZP like alpha-2-macroglobulin domain containing 8; early growth response 1

Introduction

Ovarian cancer (OC) is the second leading cause of gynecological cancer-related mortality in women. Over 70% of patients are diagnosed at an advanced stage, and most experience relapse within three years [1,2]. Currently, cytoreductive surgery combined with chemotherapy remains the standard treatment for advanced OC. In high-risk patients, molecular targeted therapies are employed to improve prognosis [3].

The targeted drugs Olaparib and Niraparib are highly effective selective inhibitors of *poly(ADP-ribose) polymerase (PARP) 1* and *PARP2*. They are commonly used in clinical settings for patients with *BRCA1/2* mutations (BRCA1/2mut) or as adjuvant therapy for advanced platinum-sensitive, relapsed OC, significantly prolonging progression-free survival (PFS) [3]. For instance, Niraparib extends PFS in patients with *BRCA1* mutations, homologous recombination (HR) deficiency (HRD), and wild-type *BRCA* (BRCAwt) from 3.9 months to 15.5, 11.5, and 9.3 months, respectively [4,5]. Olaparib extends PFS in *BRCA1*-mutant OC from 4.3 to 11.2 months, and in BRCAwt OC from 5.5 to 7.4 months [4]. Although Olaparib and Niraparib are effective in alleviating symptoms in OC patients, more than half of the patients still show weak responses to these therapies, and ultimately, most experience tumor recurrence or metastasis [4].

Most studies have focused on understanding the mechanisms of PARPis resistance by examining genomic changes in OC cells after drug stimulation. Various functional genomic approaches have been employed to identify molecular targets or combination strategies that could enhance the response to PARPis treatment, guiding the development of clinical PARPis [6]. For example, Liu M *et al.* [7] constructed four chronic stress OC mouse models and identified several genes in the glycolysis and DNA damage pathways associated with Niraparib and platinum resistance. Biegała Ł *et al.* [8] developed an Olaparib-resistant OC cell line and discovered that *miR-99b-5p*, *miR-424-3p*, *miR-505-5p*, and *miR-324-5p* were associated with Olaparib resistance or relapse, clarifying the regulatory role of growth factor expression in this process. Previous studies have confirmed that PARPis resistance is linked to the restoration of HR repair due to *BRCA1* restoration mutations and replication fork stabilization [9]. Genome sequencing by Waks AG and others [10] further confirmed changes in the HR genome following DNA damage in PARPis-resistant tumor samples. Furthermore, Tan J *et al.* [11] showed that C/EBPβ regulates HR genes to promote PARPis resistance and that targeting C/EBPβ induces HRD, rescuing PARPis sensitivity. Zhang X *et al.* [12] induced polyploid giant cancer cell (PGCC) formation in Olaparib-acquired resistance OC cell lines, high-grade serous carcinoma (HGSC)-derived organoids, and patient-derived xenografts (PDX). Additionally, transcriptomic analysis revealed that the downregulation of cell proliferation-related pathways in PGCC plays a key role in Olaparib resistance [12]. These studies together have provided important insights into the mechanisms underlying PARPis resistance through transcriptomic changes in drug-resistant OC models.

However, most models in these studies are based on pre-established drug-resistant cell lines or clinically acquired drug-resistant tumor tissues [13], directly investigating genomic changes in resistant samples, but lacking a temporal perspective. To address this, the current study treated OC cell lines with PARPis at different time points and analyzed the transcriptomic changes over time. This approach allows for a deeper understanding of how PARPis influences gene regulation in OC cells and helps to elucidate the temporal dynamics of gene expression in response to PARPis. Additionally, we screened for significantly differentially expressed genes (DEGs) after long-term (6-month) stimulation, validated the results using publicly available datasets from the Gene Expression Omnibus (GEO) database (https://www.ncbi.nlm.nih.gov/geo/), and identified overlapping genes as potential targets of Olaparib and Niraparib resistance. Their prognostic significance was also analyzed.

Materials and Methods

Ovarian Cancer Cell Lines Cultured With Olaparib and Niraparib at Different Time Periods

SKOV3 (SK-OV-3, Guangzhou Xinyuan Biotechnology Co., Ltd., Guangzhou, China) and OVCAR8 (OVCAR-8, Guangzhou Xinyuan Biotechnology Co., Ltd., Guangzhou, China) cells were sub-cultured in McCoy's 5A complete medium (10% fetal bovine serum (FBS) + 1% penicillin-streptomycin; Biospecies-0011, Guangzhou Xinyuan Biotechnology Co., Ltd., Guangzhou, China) and RPMI-1640 (XY-9846, Guangzhou Xinyuan Biotechnology Co., Ltd., Guangzhou, China) at 37 °C and 5% CO_2. The identity of the cell lines was confirmed by short tandem repeat (STR) sequencing, ensuring no cell line contamination. SKOV3 and OVCAR8 cells were seeded in 96-well plates at a density of 10^4 cells/well and cultured with complete medium containing 0.065% Dimethyl sulfoxide (DMSO), as well as 1, 10, 100, 500, and 1000 µM Olaparib (SST-C036, Acon Biotech (Hangzhou) Co., Ltd., Hangzhou, China) or Niraparib (SST-C038, Acon Biotech (Hangzhou) Co., Ltd., China) for 2, 3, and 7 days. Afterward, 10 µL of Cell Counting Kit-8 (CCK8) reagent (KTA1020, Abbkine (Wuhan) Biotechnology Co., Ltd., China) was added to the wells, incubated for 1 hour at 37 °C, and the absorbance at 450 nm (OD_{450}) was measured using a microplate reader (SpectraMax iD5, Molecular Devices, Shanghai, China). The cell viability (%) of the drug-treated group was calculated relative to the DMSO-treated group based on OD_{450}.

Log_{10} concentration and cell viability curves were plotted, and the half-maximal inhibitory concentration (IC_{50}) of each drug was determined. The IC_{50} values obtained after 7 days of drug treatment were used to prepare drug-containing complete medium for subsequent long-term culture of SKOV3 and OVCAR8 cells. For this, SKOV3 (SKOV3_Nira) and OVCAR8 (OVCAR8_Nira) cells were cultured for 2 (SKOV3_Nira_2M, OVCAR8_Nira_2M), 3 (SKOV3_Nira_3M, OVCAR8_Nira_3M), and 6 (SKOV3_Nira_6M, OVCAR8_Nira_6M) months in RPMI-1640 complete medium containing 50 µM McCoy's 5A medium and 21 µM Niraparib. SKOV3 cells were cultured for 2 months in McCoy's 5A medium with 60 µM Olaparib (SKOV3_Ola_2M), then the medium was replaced with 30 µM Olaparib and cultured for 1 (SKOV3_Ola_3M) and 4 months (SKOV3_Ola_6M). OVCAR8 cells were cultured for 2 (OVCAR8_Ola_2M), 3 (OVCAR8_Ola_3M), and 6 (OVCAR8_Ola_6M) months in RPMI-1640 medium containing 38 µM Olaparib. Control groups of SKOV3 (SKOV3_parent) and OVCAR8 (OVCAR8_parent) cells were cultured and passaged simultaneously in drug-free complete medium. Fresh culture medium was replaced every three days, and cells with a fusion rate exceeding 85% were passaged.

Changes in Drug Sensitivity of Ovarian Cancer Cells After Treatment With Olaparib and Niraparib at Different Time Periods

SKOV3 and OVCAR8 cells cultured for 2, 3, or 6 months with complete medium containing no drug, Olaparib, or Niraparib were collected and seeded into 96-well plates at 10^4 cells/well. Cells were cultured for 3 days with complete medium containing 0.065% DMSO and 1–1000 µM Olaparib or Niraparib. CCK8 reagent was added for 1 hour, and OD_{450} was measured to calculate cell viability, IC_{50}, and drug resistance index (RI). The formula for RI is: IC_{50} (drug-treated group) ÷ IC_{50} (drug-free group). RI values between 1 and 5 indicate mild drug resistance [14,15].

Transcriptome Expression Matrix of Ovarian Cancer Cells After Olaparib and Niraparib Treatment for the Different Time Periods

Cell cultures from the ten experimental groups yielded samples that met the following criteria for collection: a total cell count $>1 \times 10^7$ and viability exceeding 99%. Each group including SKOV3_parent, SKOV3_Nira_2M, SKOV3_Nira_3M, SKOV3_Nira_6M, SKOV3_Ola_3M, SKOV3_Ola_6M, OVCAR8_parent, OVCAR8_Nira_3M, OVCAR8_Nira_6M, and OVCAR8_Ola_6M, was established in triplicate. Raw sequencing data with a depth of 30 million reads per sample were obtained. Total RNA extraction, library construction, and paired-end transcriptome sequencing (RNA-seq) were performed with technical support from Beijing Benagen. We used fastp (v0.12.4, https://github.com/OpenGene/fastp, OpenGene, HaploX Biotechnology Co., Ltd., Shenzhen, China) for quality control of the sequences, and Bowtie2 (v2.2.5, https://github.com/BenLangmead/bowtie2, Baltimore, MD, USA) to align high-quality sequences to the human GRCh38 reference genome. Samtools (v1.3.1, https://github.com/samtools/samtools) was used to process BAM files (view, index, and sort), and the gene counting tool featureCounts (v2.0.1) in Subread (SourceForge, San Diego, CA, USA) was employed to obtain the total number of reads mapped to each gene. The median values for total sequencing reads, GC content, Q20, and Q30 ratios across all samples were 58,850,359 (41,318,000~79,933,696, **Supplementary Fig. 1A**), 0.472 (0.466~0.480, **Supplementary Fig. 1B**), 0.991 (0.988~0.994, **Supplementary Fig. 1C**), and 0.974 (0.967~0.981, **Supplementary Fig. 1D**), respectively. These sequencing metrics indicate that the data are of sufficient quality for subsequent analyses. The gene quantification results for all samples were merged, converted to log_2 Transcripts Per Million+1 (log_2 TPM+1) values for normalization. The expression values were consistently within the range of 0 to 8, with no noticeable outliers (**Supplementary Fig. 1E**). Dimensionality reduction and cluster analysis based on the log_2(TPM+1) values revealed significant separation between the OVCAR8 and SKOV3 samples, suggesting that these two cell lines exhibit distinct transcriptional profiles (**Supplementary Fig. 1F,G**).

$$A = \frac{\text{Count} \times 10^3}{\text{gene length}}$$

$$\log_2(TPM+1) = \log_2\left(\frac{A}{\Sigma A} \times 10^6 + 1\right)$$

Discreteness and Clustering of Ovarian Cancer Cell Samples Based on Transcriptome Expression After Olaparib and Niraparib Treatment

Principal component analysis (PCA) was performed using the R packages "FactoMineR" (v2.11, https://github.com/husson/FactoMineR) and "factoextra" (v1.0.7, https://github.com/kassambara/factoextra) to assess sample discreteness across groups. Euclidean distances were calculated using the dist function in R (v4.2.1), followed by hierarchical clustering with the hclust function (method = "complete") to examine the similarity of transcriptome expression among the samples.

Significantly Differentially Expressed Genes and Functional Enrichment Analysis

DEGs were identified using the "limma" package (v3.54.2, https://bioinf.wehi.edu.au/limma/) based on comparisons of each group to the SKOV3_parent or OVCAR8_parent control groups. DEGs were selected using a threshold of adjusted p-value < 0.05 and $|\log_2$ fold

change| >1. Functional enrichment analysis was conducted using the "clusterProfiler" (v4.4.4, https://bioconductor.org/packages/clusterProfiler/) and "org.Hs.eg.db" (v3.15.0, https://bioconductor.org/packages/org.Hs.eg.db/) packages for Gene Ontology (GO) terms (biological process, cellular component, and molecular function) and Kyoto Encyclopedia of Genes and Genomes (KEGG) pathways. Gene set enrichment analysis (GSEA) was performed using GSEABase (v1.60.0, https://bioconductor.org/packages/GSEABase/).

Interaction Analysis of Key Genes in Ovarian Cancer Cell Samples After Olaparib and Niraparib Treatment

Protein-protein interaction (PPI) networks were constructed for DEGs using the public database String (v12.0, https://string-db.org/) and Cytoscape software (v3.9.1, Institute for Systems Biology, Washington D.C., USA). The top 10 core nodes in the PPI network were identified using the cytohubba plugin (Maximal Clique Centrality algorithm, MCC), and the core protein clusters (k score >3) were obtained using the Molecular Complex Detection (MCODE) plugin in Cytoscape.

Consistency Analysis of Expression Trends of DEGs in Other Ovarian Cancer Datasets

We obtained Niraparib resistance-related Olaparib short-term treatment or resistance cell models from the GEO database (Table 1). DEGs from these datasets were compared with DEGs identified in our study for overlapping trends.

Further Screening of Significantly Differentially Expressed Genes and Their Correlation With Survival Prognosis

In this step, Cox regression analysis was performed on multiple DEGs using the Sur and coxph functions from the R packages "survival" (v3.6-4, https://github.com/therneau/survival) and "survminer" (v0.4.9, https://github.com/kassambara/survminer). We statistically analyzed the hazard ratio (HR) and 95% confidence interval (CI) for each DEG with respect to overall survival (OS) time (in days), OS status, disease-free survival (DFS) time, and DFS status. Additionally, the survfit function was used to perform Kaplan-Meier survival analysis for each DEG.

Real-Time Quantitative Polymerase Chain Reaction

Total RNA was subsequently isolated from SKOV3_parent, SKOV3_Nira_6M, SKOV3_Ola_6M, OVCAR8_parent, OVCAR8_Nira_6M, and OVCAR8_Ola_6M cells using a commercial RNA extraction kit (DP451-TA, Tiangen, Beijing, China) and reverse-transcribed into cDNA with the StarScript III one-tube kit (A230-02, GeneStar, Beijing, China). Quantitative PCR (qPCR) was performed using a 2× RealStar Fast SYBR mix (A301-01, GeneStar, Beijing, China) and gene-specific primers for *CPAMD8* (F: 5′-TTAACTCTCCAAGGGAAGTCACG-3′; R: 5′-GGTCTGGTTGTGAAAGAGGGG-3′), *EGR1* (F: 5′-GGTCAGTGGCCTAGTGAGC-3′; R: 5′-GTGCCGCTGAGTAAATGGGA-3′), and the endogenous control *GAPDH* (F: 5′-GGAGCGAGATCCCTCCAAAAT-3′; R: 5′-GGCTGTTGTCATACTTCTCATGG-3′). Relative mRNA expression levels were normalized to GAPDH and calculated using the $2^{-\Delta\Delta Cq}$ method.

Western Blotting

Total protein was isolated from SKOV3_parent, SKOV3_Nira_6M, SKOV3_Ola_6M, OVCAR8_parent, OVCAR8_Nira_6M, and OVCAR8_Ola_6M cells using TRIzol reagent (15596026CN, Thermo Fisher Scientific, Waltham, MA, USA). Protein concentrations were determined by a bicinchoninic acid (BCA) assay (KTD3001, LaiSai Bio, Guangzhou, China). For each sample, 20 µg of total protein was resolved electrophoretically on 8% or 10% SDS-polyacrylamide gel (PG112, Shanghai Yamei Biomedical Technology, Shanghai, China) under constant voltage: 80 V for the initial 20 min, followed by 120 V until the dye front reached the bottom of the gel. The separated proteins were subsequently transferred onto a 0.22 µM nitrocellulose membrane via wet transfer at 200 mA for 100 min at 4 °C. After transfer, the membrane was blocked with 5% bovine serum albumin (BSA, A1933-25G, Sigma, Burlington, MA, USA) for 2 h. Immunoblotting was performed by incubating the membrane with specific primary antibodies (CPAMD8 antibody, 0.5 µg/mL, PA5-114401, Thermo Fisher Scientific, Waltham, MA, USA; EGR1 antibody, 1:50,000; ab194357, Abcam, Cambridge, MA, USA) at 4 °C overnight, followed by incubation with appropriate horseradish peroxidase (HRP)-conjugated secondary antibody (goat anti-rabbit IgG, 1:20,000; ab205718, Abcam, Cambridge, MA, USA) for 1 hour. Protein bands were detected using an enhanced chemiluminescence (ECL) substrate (WBKLS0500, Sigma, Burlington, MA, USA) and imaged accordingly.

Plasmid Construction for CPAMD8 and EGR1 Overexpression

The coding sequences (CDS) of human *CPAMD8* (CCDS42519.2) and *EGR1* (CCDS4206.1) were chemically synthesized. The lentiviral overexpression vector, pLenti-CMV-GFP-Puro (17448, Addgene, Watertown, MA, USA), was double-digested with BamHI (R3136S, NEB, Ipswich, MA, USA) and SalI (R3138S, NEB, Ipswich, MA, USA) restriction enzymes to generate compatible ends for subsequent cloning. The digestion reaction was incubated according to the manufacturer's instructions, and the linearized vector was purified from an agarose gel. The synthesized CDS fragments were then ligated into the

Table 1. Related ovarian cancer datasets from the Gene Expression Omnibus public database included in the study.

GEO id	Sample type	Control group	Drug-treated group	Drug	Linked website
GSE153867	A2780	8	8	Olaparib (resistance)	https://www.ncbi.nlm.nih.gov/geo/query/acc.cgi?acc=GSE153867
GSE229119	SKOV3	1	3	Olaparib (3∼7 d)	https://www.ncbi.nlm.nih.gov/geo/query/acc.cgi?acc=GSE229119
GSE235980	UWB1.289	2	2	Olaparib (resistance)	https://www.ncbi.nlm.nih.gov/geo/query/acc.cgi?acc=GSE235980
GSE235980	UWB1.289_BRCA1	2	2	Olaparib (resistance)	https://www.ncbi.nlm.nih.gov/geo/query/acc.cgi?acc=GSE235980

GEO, Gene Expression Omnibus.

Table 2. Changes in drug resistance index (RI) of two ovarian cancer cell lines during 6 months of continuous culture with Niraparib and Olaparib.

Drug	Group / Months	Index	2		3		6	
			48 h	72 h	48 h	72 h	48 h	72 h
Niraparib	SKOV3_parent -*vs*- SKOV3_Nira	IC_{50}	29.68 ± 2.44 -*vs*- 39.24 ± 6.50	16.47 ± 1.41 -*vs*- 20.62 ± 4.15	36.55 ± 0.56 -*vs*- 46.69 ± 0.47	29.72 ± 1.26 -*vs*- 30.47 ± 1.56	40.37 ± 1.08 -*vs*- 70.97 ± 0.98	38.15 ± 5.88 -*vs*- 78.36 ± 7.70
		RI	1.32	1.25	1.28	1.03	1.76	2.05
		p	0.076	0.18	<0.0001	0.55	<0.0001	0.00052
	OVCAR8_parent -*vs*- OVCAR8_Nira	IC_{50}	43.30 ± 10.47 -*vs*- 60.46 ± 4.24	47.53 ± 20.72 -*vs*- 28.62 ± 0.30	130.95 ± 1.10 -*vs*- 130.91 ± 0.45	212.02 ± 5.81 -*vs*- 221.29 ± 5.79	97.17 ± 14.85 -*vs*- 94.23 ± 3.95	174.63 ± 5.76 -*vs*- 140.18 ± 10.68
		RI	1.40	0.60	1.00	1.04	0.97	0.80
		p	0.058	0.19	0.96	0.12	0.76	0.0080
Olaparib	SKOV3_parent -*vs*- SKOV3_Ola	IC_{50}	273.68 ± 38.49 -*vs*- 322.35 ± 9.61	165.24 ± 5.58 -*vs*- 196.05 ± 18.40	368.16 ± 8.38 -*vs*- 671.85 ± 14.01	207.96 ± 4.66 -*vs*- 207.67 ± 3.88	525.34 ± 4.17 -*vs*- 1054.23 ± 100.70	208.47 ± 12.48 -*vs*- 544.01 ± 1.24
		RI	1.18	1.19	1.82	1.00	2.01	2.61
		p	0.10	0.050	<0.0001	0.94	0.00081	<0.0001
	OVCAR8_parent -*vs*- OVCAR8_Ola	IC_{50}	477.72 ± 14.49 -*vs*- 667.59 ± 16.88	313.71 ± 58.39 -*vs*- 257.37 ± 90.30	515.84 ± 9.91 -*vs*- 539.85 ± 18.65	464.97 ± 5.89 -*vs*- 464.96 ± 16.54	680.89 ± 13.50 -*vs*- 1376.08 ± 21.71	532.35 ± 14.79 -*vs*- 1096.72 ± 34.08
		RI	1.40	0.82	1.05	1.00	2.02	2.06
		p	0.00012	0.42	0.12	1.00	<0.0001	<0.0001

pLenti-CMV-GFP-Puro vector backbone using T4 DNA ligase (M0202V, NEB, Ipswich, MA, USA) at a molar ratio of 3:1 to favor the insertion event. The ligation mixture was transformed into competent *E. coli* cells (D1031S, Beyotime, Shanghai, China). Positive clones were selected on LB agar plates (ST164, Beyotime, Shanghai, China) containing ampicillin (A5354, Sigma, Burlington, MA, USA) and further verified by colony PCR and Sanger sequencing to confirm the correct insertion and frame of the target genes. The linearized pLenti-CMV-GFP-Puro vector, obtained via double enzyme digestion, was self-ligated to generate an empty vector (ovNC) for use as a control in subsequent studies.

Cell Proliferation Assay

SKOV3_Nira_6M and OVCAR8_Nira_6M cells were treated with 45 μM or 75 μM Niraparib for three days. Similarly, SKOV3_Ola_6M and OVCAR8_Ola_6M cells were exposed to 250 μM or 500 μM Olaparib for the same duration. During this period, SKOV3 cell models were concurrently transfected with either *CPAMD8*-targeting siRNA sequences (siRNA-1: 5′-GACCTTCAAGCCCTTCTTCGTGG-3′; siRNA-2: 5′-TGGAGAAACCGATTCGTTTAAC-3′) or the overexpression plasmid pLenti-CMV-GFP-*CPAMD8* CDS (ov*CPAMD8*). In parallel, OVCAR8 cells in each group were transfected with *EGR1*-targeting siRNA-1 (5′-CGGTTACTACCTCTTATCCATCC-3′), siRNA-2 (5′-CAGGACAATTGAAATTTGCTAAA-3′), or the pLenti-CMV-GFP-*EGR1* CDS vector (ov*EGR1*). Following the 3-day incubation, all treated cells were fixed with 4% paraformaldehyde (P0099, Beyotime, Shanghai, China) at 25 °C for 30 min, washed three times with phosphate-buffered saline (PBS, Bios-P4202, Guangzhou Xinyuan Biotechnology Co., Ltd., Guangzhou, China), and stained with 0.5% crystal violet solution (G5447, SmartBuffers, Foshan, China) for 10 min. After air-drying, the stained cells were imaged under an optical microscope (DMiL, Leica Microsystems GmbH, Wetzlar, Hessen, Germany). Furthermore, cell suspensions from each aforementioned group were mixed with 0.4% Trypan blue (C0011S, Beyotime, Shanghai, China) stain at a 1:1 ratio, incubated at 25 °C for 5 min, and then counted using an automated cell counter (TC20™, BD, Franklin Lakes, NJ, USA) to calculate cell viability.

Statistical Methods

All statistical analyses were performed using GraphPad Prism 10 (GraphPad Software, Boston, MA, USA) and R (v4.2.1, The R Foundation for Statistical Computing, Vienna, Austria), along with the RStudio Server (v2023.09.01, Posit Software, Boston, MA, USA) for visualization. Differential gene expression between two groups was assessed using the empirical Bayes method, with *p*-values adjusted using the Benjamini-Hochberg (BH) correction. Functional enrichment analysis of DEGs was conducted using the hypergeometric distribution test. The Pearson correlation coefficient was analyzed using a *t*-test. The Cox regression risk model was evaluated using the likelihood ratio test, and Kaplan-Meier (K-M) survival curves were compared using the Log-rank test. For the IC_{50} and cell viability data, two-way analysis of variance (ANOVA) and Tukey's multiple comparisons test were applied to compare differences between multiple groups. Statistical significance was defined as a p-value < 0.05.

Results

Ovarian Cancer Cells Cultured for 6 Months Develop Mild Resistance to Olaparib and Niraparib

We first determined the IC_{50} values of SKOV3 and OVCAR8 cells after culture with varying concentrations of Niraparib or Olaparib for 7 days. These cells were subsequently cultured in complete medium containing half of the IC_{50} concentration of Niraparib or Olaparib for 2, 3, and 6 months, as shown in Fig. 1A.

Although the drug RI for each group of cells against Olaparib and Niraparib remained below 3 (Table 2), we observed a significant increase in the IC_{50} of SKOV3 cells over time with Niraparib treatment (Fig. 1B,C and **Supplementary Fig. 2A–L**). Specifically, the IC_{50} of SKOV3 cells after 6 months of Niraparib culture (SKOV3_Nira_6M, 78.36 ± 7.70 μM) was significantly higher than that of the SKOV3_parent group (38.15 ± 5.88 μM) at 72 h (RI = 2.05, $p < 0.0001$; Table 2, Fig. 1C, and **Supplementary Fig. 2K**). For Olaparib (Table 2, Fig. 1D,E, and **Supplementary Fig. 3A–L**), the IC_{50} for the SKOV3_Ola_6M group (1054.23 ± 100.70 μM; Table 2 and **Supplementary Fig. 3I**) was significantly greater than the SKOV3_parent group (368.16 ± 8.38 μM at 3 months; 525.34 ± 4.17 μM at 6 months; Table 2 and **Supplementary Fig. 3E,I**) at 48 h (RI = 1.82 or 2.01, $p < 0.001$; Table 2 and Fig. 1D). Similarly, the IC_{50} of SKOV3_Ola_6M at 72 h also increased significantly (208.47 ± 12.48 -*vs*- 544.01 ± 1.24 μM, RI = 2.61, $p < 0.0001$; Table 2, Fig. 1E, and **Supplementary Fig. 3K**).

In contrast, OVCAR8 cells cultured with Niraparib for 6 months showed no significant change, or even a decreasing trend in IC_{50} compared with the OVCAR8_parent group at 48 h (RI = 0.97, 97.17 ± 14.85 -*vs*- 94.23 ± 3.95 μM, $p > 0.05$; Table 2 and **Supplementary Fig. 2J**) or 72 h (RI = 0.80, 174.63 ± 5.76 -*vs*- 140.18 ± 10.68 μM, $p < 0.01$; Table 2, Fig. 1F,G, and **Supplementary Fig. 2L**). However, the IC_{50} values of Olaparib for OVCAR8_Ola_6M cells at 48 h (RI = 2.02, 680.89 ± 13.50 -*vs*- 1376.08 ± 21.71 μM, $p < 0.001$) and 72 h (RI = 2.06, 532.35 ± 14.79 -*vs*- 1096.72 ± 34.08 μM, $p < 0.0001$; Table 2, Fig. 1H,I, and **Supplementary Fig. 3L**) were significantly higher than those of the OVCAR8_parent group.

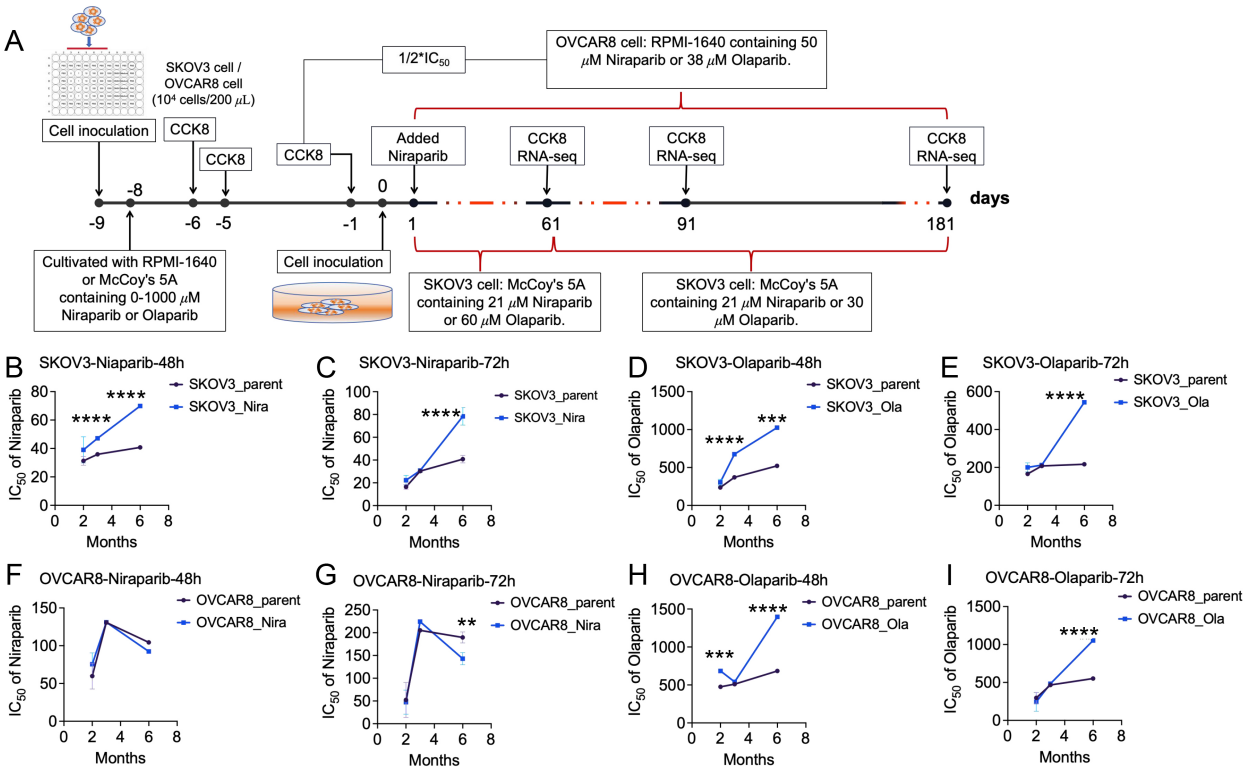

Fig. 1. Changes in drug sensitivity of ovarian cancer cell lines after culture with two poly(ADP-ribose) polymerase (PARP) inhibitors for different durations. (A) Schematic diagram of continuous culture of SKOV3 and OVCAR8 cell lines with half of the IC_{50} concentration of Niraparib and Olaparib. (B,C) Niraparib sensitivity of SKOV3 cells at 48 (B) and 72 (C) h after continuous culture with 0–1000 µM Niraparib for 2, 3, and 6 months. (D,E) Changes in the IC_{50} of SKOV3 cells at 48 (D) and 72 (E) h after continuous culture with 0–1000 µM Olaparib for 2, 3, and 6 months. (F,G) Changes in drug sensitivity of OVCAR8 cells at 48 h (F) and 72 h (G) after long-term culture with Niraparib for 2, 3, and 6 months. (H,I) Changes in drug sensitivity of OVCAR8 cells at 48 h (H) and 72 h (I) after long-term culture with Olaparib for 2, 3, and 6 months. IC_{50}, half-maximal inhibitory concentration; CCK8, Cell Counting Kit-8; RNA-seq, ribonucleic acid sequencing; OVCAR8_parent, OVCAR8 cells cultured without drugs; OVCAR8_Nira, OVCAR8 cells treated with Niraparib; OVCAR8_Ola, OVCAR8 cells treated with Olaparib; SKOV3_parent, SKOV3 cells cultured without drugs; SKOV3_Nira, SKOV3 cells treated with Niraparib; SKOV3_Ola, SKOV3 cells treated with Olaparib. **, *** and **** denote comparisons with the drug-free treatment group,with p values < 0.01, 0.001 and 0.0001, respectively.

These results suggest that SKOV3 cells, cultured with Olaparib or Niraparib for 6 months, develop mild resistance to both drugs. In contrast, OVCAR8 cells exhibit mild resistance to Olaparib but no significant change in sensitivity to Niraparib after 6 months of treatment.

162 Genes Show Differential Expression in Ovarian Cancer Cells After Long-Term Culture With Olaparib and Niraparib

After 6 months of PARPis culture, most SKOV3 and OVCAR8 cells exhibited significantly lower drug sensitivity compared with their untreated parental controls (SKOV3_parent, OVCAR8_parent) (Table 2 and Fig. 1). Given this notable shift, we focused on characterizing the morphological and transcriptomic changes in these long-term treated groups and observed morphological changes in the cells after 6 months of drug treatment (Fig. 2A). SKOV3_parent cells exhibited clear boundaries and epithelial-like adherent growth with tight cell-cell contact. However, SKOV3_Nira_6M and SKOV3_Ola_6M cells showed enlarged cell bodies and nuclei, with extended cell processes (Fig. 2A). In contrast, OVCAR8_parent cells appeared round and adhered in sheet-like clusters. After long-term treatment with Niraparib and Olaparib (OVCAR8_Nira_6M and OVCAR8_Ola_6M), cell morphology remained largely unchanged, but the cells grew more slowly, with increased cell debris and more sparse distribution. These results suggest that SKOV3 cells developed mild resistance to both PARPis, whereas OVCAR8 cells showed no substantial morphological changes.

Regarding cell viability, SKOV3_Nira_6M cells treated with Niraparib (1, 10, and 100 µM) exhibited significantly higher viability than SKOV3_parent cells ($p <$ 0.0001, Fig. 2B). Similarly, SKOV3_Ola_6M cells treated with 500 and 1000 µM Olaparib had significantly reduced viability compared with the SKOV3_parent group

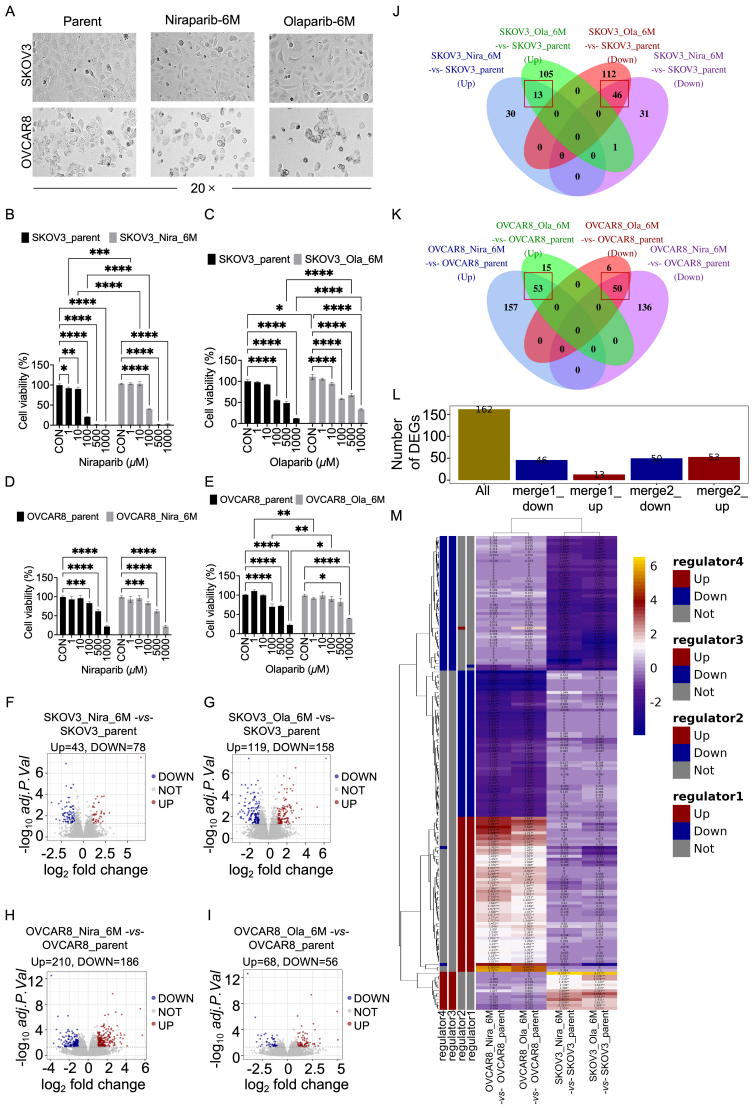

Fig. 2. Morphological changes and differential gene expression in ovarian cancer cells after long-term culture with Olaparib and Niraparib for 6 months. (A) Representative images of cell morphology and status of SKOV3 and OVCAR8 cells under the microscope (20×). (B–E) Changes in cell viability in SKOV3_Nira_6M (B), SKOV3_Ola_6M (C), OVCAR8_Nira_6M (D), and OVCAR8_Ola_6M (E) cells after treatment with different concentrations of Niraparib and Olaparib, measured using the Cell Counting Kit-8 (CCK8) assay. (F–I) Gene expression differences between SKOV3_Nira_6M (F), SKOV3_Ola_6M (G), OVCAR8_Nira_6M (H), and OVCAR8_Ola_6M (I) cells compared with their parental counterparts. (J) Venn diagram showing the overlapping differentially expressed genes (DEGs) in SKOV3_Nira_6M (*-vs-* SKOV3_parent) and SKOV3_Ola_6M (*-vs-* SKOV3_parent). (K) Venn diagram showing the overlapping DEGs in OVCAR8_Nira_6M (*-vs-* OVCAR8_parent) and OVCAR8_Ola_6M (*-vs-* OVCAR8_parent). (L) Bar chart showing the number of DEGs with consistent expression trends after 6 months of treatment with Niraparib and Olaparib. (M) Fold changes in the differential expression of selected DEGs in OC cells across different treatment groups. Merge1_up, DEGs that are upregulated in both SKOV3_Nira_6M and SKOV3_Ola_6M; merge1_down, DEGs that are downregulated in both SKOV3_Nira_6M and SKOV3_Ola_6M; merge2_up, DEGs that are upregulated in both OVCAR8_Nira_6M and OVCAR8_Ola_6M; merge2_down, DEGs that are downregulated in both OVCAR8_Nira_6M and OVCAR8_Ola_6M; OVCAR8_parent, Parental OVCAR8 cells cultured without drugs; OVCAR8_Nira_3M/OVCAR8_Nira_6M, OVCAR8 cells treated with Niraparib for 3 or 6 months; OVCAR8_Ola_6M, OVCAR8 cells treated with Olaparib for 6 months; SKOV3_parent, Parental SKOV3 cells cultured without drugs; SKOV3_Nira_2M/SKOV3_Nira_3M/SKOV3_Nira_6M, SKOV3 cells treated with Niraparib for 2, 3, or 6 months; SKOV3_Ola_3M/SKOV3_Ola_6M, SKOV3 cells treated with Olaparib for 3 or 6 months. * $p < 0.05$, ** $p < 0.01$, *** $p < 0.001$, **** $p < 0.0001$.

Table 3. Number of signaling pathways significantly enriched in significantly differentially expressed genes ($q < 0.05$).

Ontology	Biological processes	Molecular functions	Cellular Component	KEGG pathway
Merge1_up (n = 13)	3	0	0	0
Merge1_down (n = 46)	11	0	0	0
Merge2_up (n = 53)	37	21	1	0
Merge2_down (n = 50)	0	0	0	0
Union (n = 162)	20	0	4	0

Merge1_up, DEGs that are upregulated in both SKOV3_Nira_6M and SKOV3_Ola_6M; merge1_down, DEGs that are downregulated in both SKOV3_Nira_6M and SKOV3_Ola_6M; merge2_up, DEGs that are upregulated in both OVCAR8_Nira_6M and OVCAR8_Ola_6M; merge2_down, DEGs that are downregulated in both OVCAR8_Nira_6M and OVCAR8_Ola_6M; KEGG, Kyoto Encyclopedia of Genes and Genomes.

($p < 0.0001$, Fig. 2C). In contrast, no significant differences were observed between OVCAR8_Nira_6M and OVCAR8_parent cells treated with Niraparib at the same concentrations ($p > 0.05$, Fig. 2D). However, the OVCAR8_Ola_6M group exhibited significantly lower viability after treatment with 100, 500, and 1000 µM Olaparib compared with OVCAR8_parent cells ($p < 0.05$, Fig. 2E). These findings suggest that both SKOV3 and OVCAR8 cells developed some degree of resistance to Olaparib after long-term treatment, with SKOV3 cells also showing resistance to Niraparib, while OVCAR8's response to Niraparib remained largely unchanged. Despite no significant changes in Niraparib sensitivity, the transcriptomic profiles of OVCAR8_Nira_6M cells clustered with the mildly resistant OVCAR8_Ola_6M group, highlighting similar gene expression changes (**Supplementary Fig. 1F,G**).

We identified 121 DEGs in SKOV3 cells mildly resistant to Niraparib (Fig. 2F) and 277 DEGs in SKOV3 cells resistant to Olaparib through transcriptome sequencing and analysis (Fig. 2G). In OVCAR8 cells, long-term treatment with Niraparib and Olaparib resulted in 396 (Fig. 2H) and 124 (Fig. 2I) DEGs, respectively. Among the 162 overlapping DEGs identified in both SKOV3 and OVCAR8 cells after long-term treatment with the two drugs, 96 were downregulated and 66 were upregulated (Fig. 2J–M).

Among the 162 overlapping DEGs, 13 genes consistently upregulated in SKOV3 after long-term stimulation were enriched in three BP terms, including processes related to the respiratory system development (Fig. 3A and **Supplementary Table 1**). Conversely, 46 DEGs consistently downregulated in SKOV3 were enriched in 11 BP terms, mainly related to epithelial cell development, intracellular estrogen receptor signaling, and intermediate filament assembly (Fig. 3B and **Supplementary Table 1**). In OVCAR8 cells, 53 DEGs consistently upregulated after drug treatment were significantly enriched in 37 BP terms and 21 MF terms, primarily related to multi-organism reproduction, female pregnancy, positive regulation of epithelial cells, and plasma membrane adhesion (Fig. 3C and **Supplementary Table 1**). The majority of these upregulated genes had functions in receptor signaling, ligand-receptor interaction, and cytokine activity. In contrast, 50 DEGs consistently downregulated in OVCAR8 cells were primarily non-coding RNAs and lacked significantly enriched biological functions (Table 3).

These results demonstrate that long-term treatment with Olaparib and Niraparib induces consistent changes in gene expression across both SKOV3 and OVCAR8 cells, although there are notable differences between the two cell lines. These differences may be attributed to inherent variations in transcriptomic profiles and cellular responses to drug exposure.

97 Genes Showed Consistent Significant Differential Expression in Both Medium- and Long-Term Drug Stimulation Periods

We further analyzed the similarities and differences in the transcriptomic changes of SKOV3 and OVCAR8 cells after stimulation with two types of PARPis for different durations. The results revealed that 162 DEGs were consistently differentially expressed after 6 months of long-term drug stimulation. The differential expression at other time points (2 months or 3 months) is shown in Fig. 4A,B. At these time points, 97 DEGs were identified, including 22 upregulated DEGs (22up-DEGs, Fig. 4C) and 75 downregulated DEGs (75down-DEGs, Fig. 4D). These 22 upregulated and 75 downregulated DEGs were integrated into a PPI network, with estrogen receptor 1 (*ESR1*) as the core (Fig. 5A), and were significantly enriched in BP terms related to epithelial development and differentiation (Fig. 5B and **Supplementary Table 2**).

Further analysis revealed that the following genes were also identified as core nodes of the PPI network: *ESR1*, *KRT14*, *KRT5*, and others (Fig. 5C). These genes were significantly up or down regulated in the following specific conditions (Table 4), and core gene clusters consisting of *ESR1*, *CDH2*, *KRT5*, and *KRT14* were identified by MCODE analysis (Fig. 5D). Notably, *FASN* and *KRT17* remained downregulated in SKOV3 cells after 2 months of Niraparib treatment, while *ABCB1*, *KRT17*, and *MME* were consistently upregulated, and *CDH2* was consistently downregulated in OVCAR8 cells exposed to PARPis (Table 4).

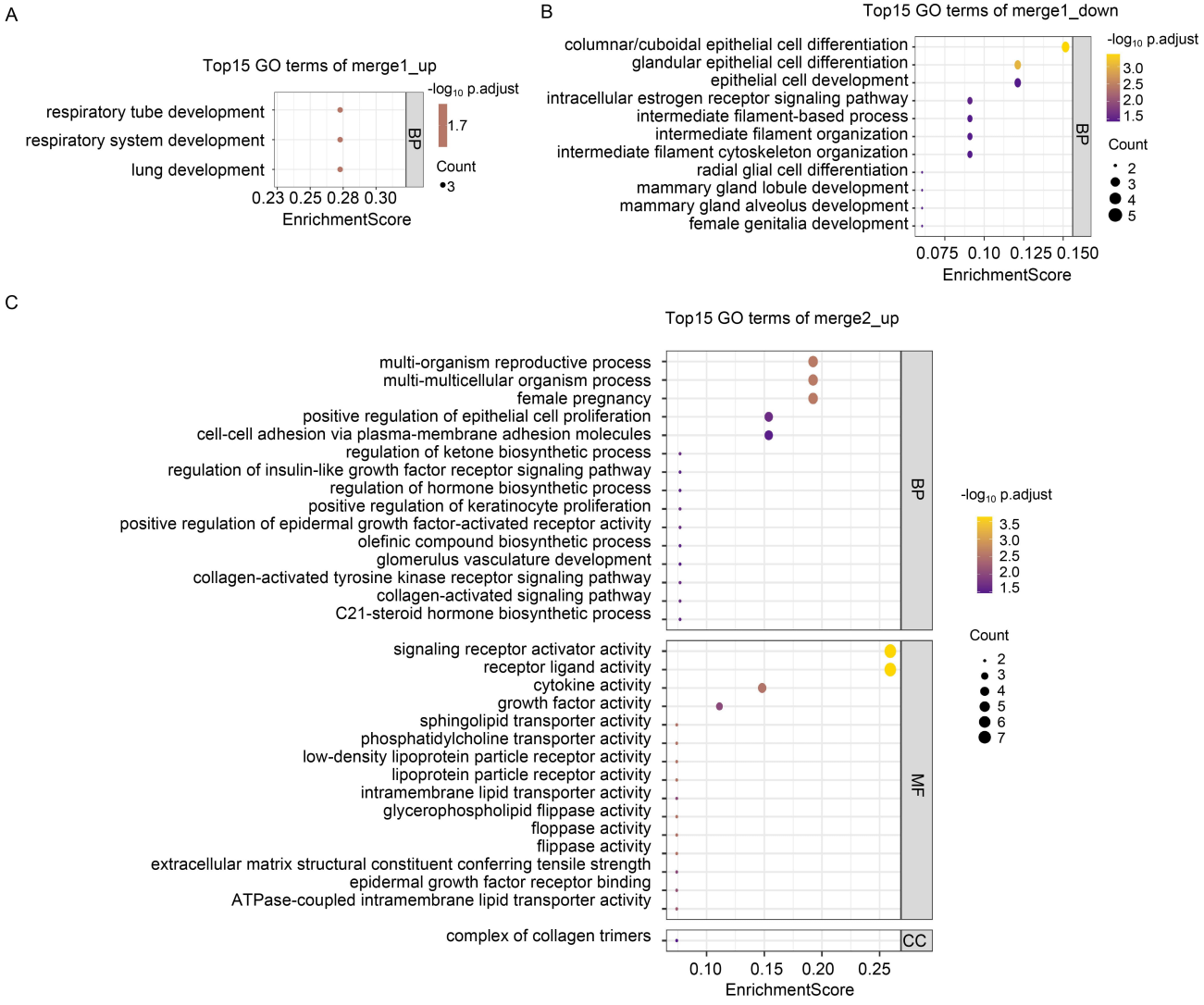

Fig. 3. Gene Ontology (GO) enrichment analysis of overlapping significantly differentially expressed genes (DEGs) in ovarian cancer cells after 6 months of Olaparib and Niraparib treatment. (A–C) Biological process (BP) and molecular function (MF) enrichment analysis of overlapping DEGs including 13 upregulated DEGs (merge1_up, A) in SKOV3 cells, 46 downregulated DEGs (merge1_down, B) in SKOV3 cells, 53 upregulated DEGs (merge2_up, C) in OVCAR8 cells. Merge1_up, DEGs that are upregulated in both SKOV3_Nira_6M and SKOV3_Ola_6M; merge1_down, DEGs that are downregulated in both SKOV3_Nira_6M and SKOV3_Ola_6M; merge2_up, DEGs that are upregulated in both OVCAR8_Nira_6M and OVCAR8_Ola_6M.

Additionally, we observed that 44up- and 21down-DEGs were enriched in biological pathways related to cell-cell adhesion (Fig. 6A and **Supplementary Table 2**). These genes showed significant differential expression in both SKOV3 and OVCAR8 cells after 6 months of PARPis treatment. However, no significant changes were observed after 2 months or 3 months of stimulation (Fig. 4). For example, in OVCAR8_Ola_6M and OVCAR8_Nira_6M, genes such as *BMP5*, *CDH3*, *COL4A1*, *COL4A2*, *DEFB103B*, *EBI3*, *EGR1*, *EPCAM*, *EPGN*, *PECAM1*, *PSG2*, *PSG5*, *PSG7*, and *PSG9* were upregulated, while GREM1 was downregulated in OVCAR8_Nira_3M. These genes are mainly involved in biological processes related to epithelial cell differentiation, epithelial growth factor receptor binding, and chemokine activation in OVCAR8 cells after 6 months of PARPis stimulation (Fig. 6B).

Furthermore, *LRRC17*, which was significantly downregulated in SKOV3_Ola_6M and SKOV3_Nira_6M, did not show significant differential expression in the SKOV3_Ola_3M, SKOV3_Nira_3M, and SKOV3_Nira_2M groups (Fig. 4B). Similarly, *CDH1* was consistently downregulated in OVCAR8_Nira_3M and OVCAR8_Ola_6M, but exhibited different expression patterns in SKOV3 cells. *CDH2* was significantly downregulated in SKOV3_Ola_6M and SKOV3_Nira_6M, but no significant changes were observed in the SKOV3_Ola_3M, SKOV3_Nira_3M, and SKOV3_Nira_2M groups.

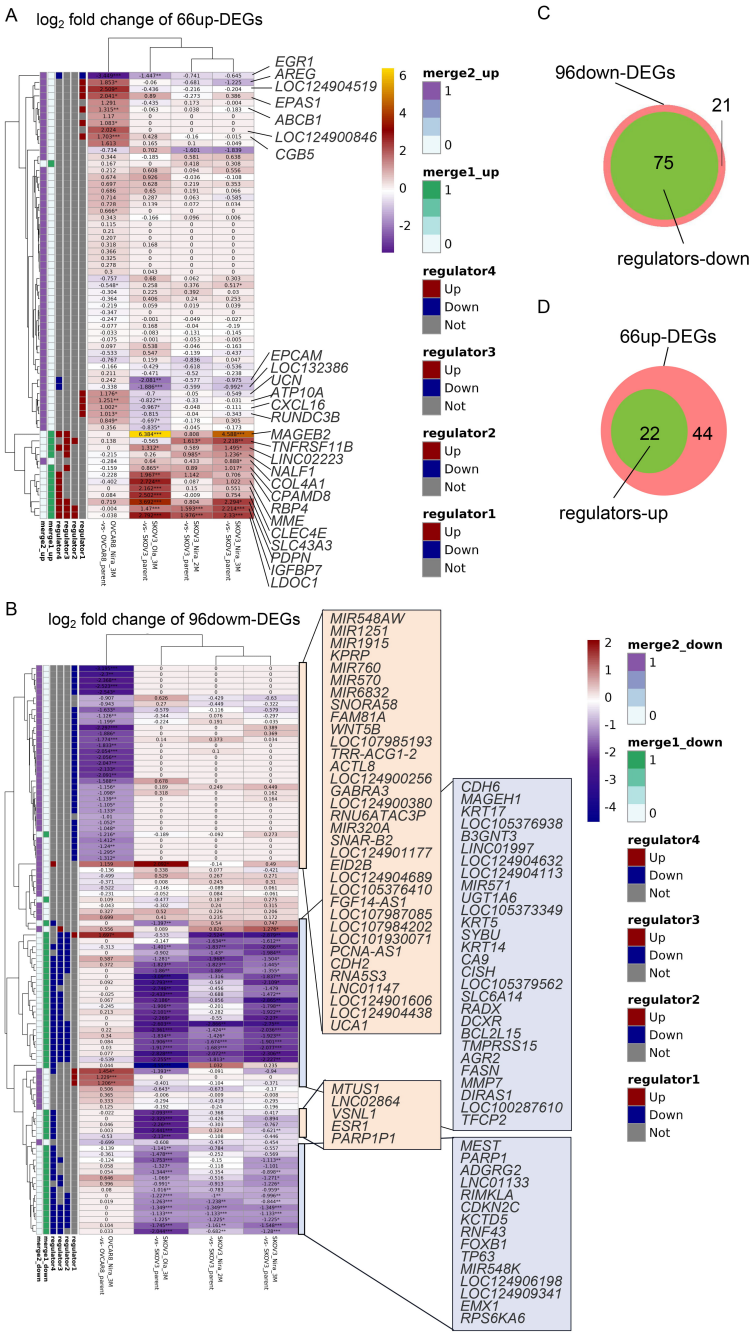

Fig. 4. Expression of 162 overlapping significantly differentially expressed genes (DEGs) after 2 or 3 months of Olaparib and Niraparib treatment. (A,B) Comparison of the differential fold change (FC) of 66 overlapping upregulated DEGs (66up-DEGs, A) and 96 overlapping downregulated DEGs (96down-DEGs, B) in SKOV3_Nira_2M, SKOV3_Nira_3M, SKOV3_Ola_3M, and OVCAR8_Nira_3M compared with their respective parental cells. (C,D) The number of consistently upregulated DEGs (C) and consistently downregulated DEGs (D) after long-term culture with Olaparib and Niraparib for 2 months, 3 months, or 6 months. Regulator1, Differential expression of genes between OVCAR8_Ola_3M and OVCAR8_parent cells; regulator2, Differential expression of genes between SKOV3_Nira_2M and SKOV3_parent cells; regulator3, Differential expression of genes between SKOV3_Nira_3M and SKOV3_parent cells; regulator4, Differential expression of genes between SKOV3_Ola_3M and SKOV3_parent cells; OVCAR8_parent, Parental OVCAR8 cells cultured without drugs; OVCAR8_Nira_3M/OVCAR8_Nira_6M, OVCAR8 cells treated with Niraparib for 3 or 6 months; OVCAR8_Ola_6M, OVCAR8 cells treated with Olaparib for 6 months; SKOV3_parent, Parental SKOV3 cells cultured without drugs; SKOV3_Nira_2M/SKOV3_Nira_3M/SKOV3_Nira_6M, SKOV3 cells treated with Niraparib for 2, 3, or 6 months; SKOV3_Ola_3M/SKOV3_Ola_6M, SKOV3 cells treated with Olaparib for 3 or 6 months. $*p < 0.05$, $**p < 0.01$, $***p < 0.001$, comparing with parental cells (SKOV3_parent, OVCAR8_parent).

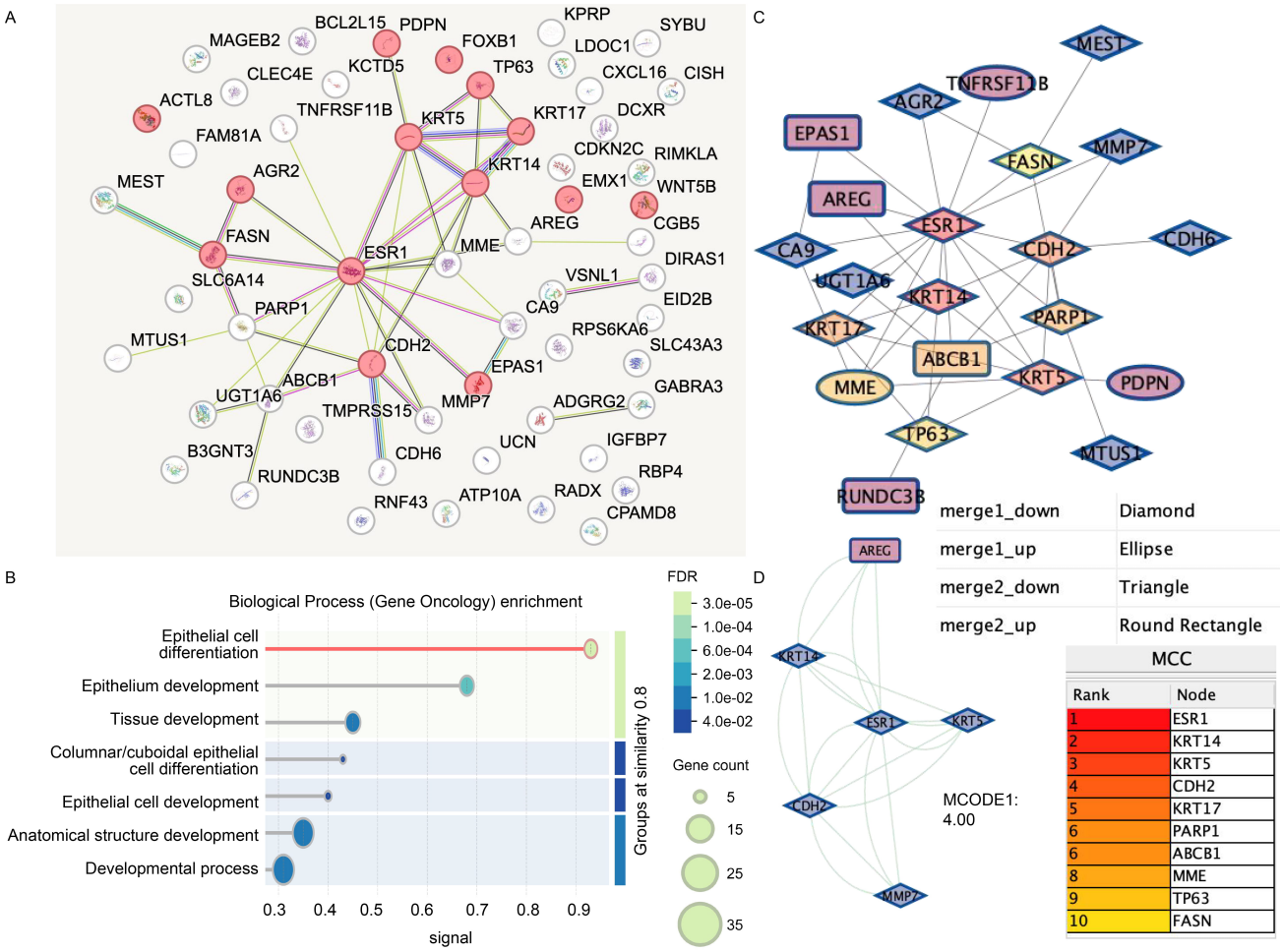

Fig. 5. Functional enrichment of 97 significantly differentially expressed genes (DEGs) with consistent trends and their interactions. (A) Protein-protein interaction (PPI) network of 97 DEGs generated using the STRING database. (B) The top 10 Gene Ontology - Biological Process (GO-BP) pathways significantly enriched by the 97 DEGs, analyzed and visualized using the STRING database. (C) Identification of the top 10 core nodes in the PPI network based on the maximum neighborhood component centrality (MCC) algorithm, calculated using the cytoHubba plugin of Cytoscape software. (D) Core clusters of the PPI network identified using the MCODE plugin of Cytoscape software. Merge1_up, DEGs that are upregulated in both SKOV3_Nira_6M and SKOV3_Ola_6M; merge1_down, DEGs that are downregulated in both SKOV3_Nira_6M and SKOV3_Ola_6M; merge2_up, DEGs that are upregulated in both OVCAR8_Nira_6M and OVCAR8_Ola_6M; merge2_down, DEGs that are downregulated in both OVCAR8_Nira_6M and OVCAR8_Ola_6M.

Significant Differential Expression of CPAMD8, DAPP1, and EGR1 After Long-Term Olaparib and Niraparib Stimulation and Their Prognostic Relevance in Ovarian Cancer

To validate the differential expression of the overlapping 162 DEGs identified after long-term PARPis stimulation, we introduced external datasets for comparison. As a result, 20 of these DEGs were significantly differentially expressed in more than one OC cell model (Fig. 7A,B, and **Supplementary Fig. 4A–E**). Among them, 13 DEGs were consistently downregulated, while 7 DEGs were consistently upregulated. For example, *PARP1*, *DCXR*, *FASN*, and *LINC01133*, which were consistently downregulated in both SKOV3_Nira_6M (**Supplementary Fig. 4A**) and SKOV3_Ola_6M (**Supplementary Fig. 4B**), were also significantly downregulated in UWB1.289_Ola_resistant and UWB1.289_BRCA1wt_Ola_resistant cells (Fig. 7C). Similarly, *MME*, which was significantly upregulated in SKOV3_Ola, was also upregulated in UWB1.289_Ola_resistant and UWB1.289_BRCA1wt_Ola_resistant groups (Fig. 7C). Additionally, *LOC643201*, which was consistently downregulated in OVCAR8_Nira_6M (**Supplementary Fig. 4C**) and OVCAR8_Ola_6M (**Supplementary Fig. 4D,E**), was also downregulated in UWB1.289 cells (Fig. 7C). *EGR1* and *EPAS1* were significantly upregulated in Olaparib-resistant A2780 cells and/or in UWB1.289 cells (Fig. 7C).

We further examined the correlation between these 20 overlapping DEGs and the prognosis of OC patients.

Table 4. The distribution of significant differential expression of the top 10 core genes in each group.

Group	Symbols ($adj.p < 0.05$ & $\|\log_2 FC\| > 1$)
SKOV3_Nira_6M	*ESR1*, *KRT14*, *KRT5*, *CDH2*, *KRT17*, *PARP1*, *TP63*, *FASN* (downregulated)
SKOV3_Ola_6M	*ESR1*, *KRT14*, *KRT5*, *CDH2*, *KRT17*, *PARP1*, *TP63*, *FASN* (downregulated)
SKOV3_Ola_3M	*ESR1*, *KRT14*, *KRT5*, *PARP1*, *TP63*, *FASN* (downregulated)
SKOV3_Nira_3M	*KRT14*, *KRT17*, *FASN* (downregulated)
SKOV3_Nira_2M	*KRT17*, *TP63*, *FASN* (downregulated)
OVCAR8_Nira_3M	*CDH2* (downregulated); *ABCB1*, *KRT17*, *MME* (upregulated)
OVCAR8_Nira_6M	*CDH2* (downregulated); *ABCB1*, *KRT17*, *MME* (upregulated)
OVCAR8_Ola_6M	*CDH2* (downregulated); *ABCB1*, *KRT17*, *MME* (upregulated)

OVCAR8_parent, Parental OVCAR8 cells cultured without drugs; OVCAR8_Nira_3M/OVCAR8_Nira_6M, OVCAR8 cells treated with Niraparib for 3 or 6 months; OVCAR8_Ola_6M, OVCAR8 cells treated with Olaparib for 6 months; SKOV3_parent, Parental SKOV3 cells cultured without drugs; SKOV3_Nira_2M/SKOV3_Nira_3M/SKOV3_Nira_6M, SKOV3 cells treated with Niraparib for 2, 3, or 6 months; SKOV3_Ola_3M/SKOV3_Ola_6M, SKOV3 cells treated with Olaparib for 3 or 6 months.

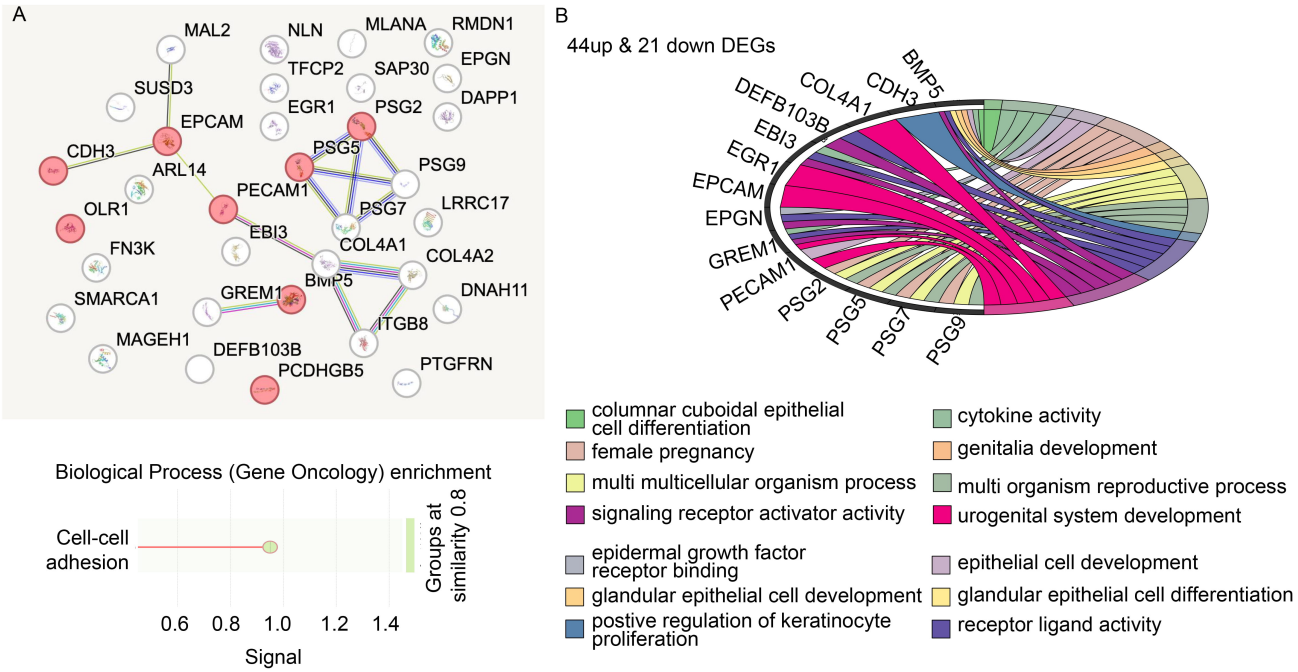

Fig. 6. Functional analysis of abnormally significant differentially expressed genes (DEGs) and their interactions in ovarian cancer cells long-term cultured with Olaparib and Niraparib for 6 months. (A) Protein-protein interaction network of 65 DEGs, along with significantly enriched biological pathways (BP), analyzed and mapped using the String database. (B) Signaling pathways and their associated genes that are significantly enriched in 65 DEGs in SKOV3 and OVCAR8 cells after long-term stimulation with Olaparib and Niraparib.

High expression levels of *CPAMD8* and *EGR1*, and low expression levels of *DAPP1*, were associated with poor OS (Fig. 7D–T). The remaining 17 DEGs did not show significant associations with OS. Additionally, expression levels of the 20 DEGs were not significantly correlated with DFS (**Supplementary Fig. 5**).

Further multivariable Cox regression analysis confirmed that histologic grade, disease stage, drug treatment, and age were significant independent prognostic factors for patient survival ($p < 0.05$; **Supplementary Table 3**), particularly for OS. Subsequent stratified analyses were performed based on these and other key parameters. Stratified Kaplan-Meier survival curves revealed that median OS was significantly worse in patients with high-grade (Grade 3; **Supplementary Fig. 6A**), advanced-stage (Stage III/IV; **Supplementary Fig. 6B**) disease, and in those who had not received initial chemotherapy/targeted therapy (**Supplementary Fig. 6C**). Interestingly, high *EGR1* expression was associated with poorer OS specifically in older patients (>64 years; **Supplementary Fig. 6D**). How-

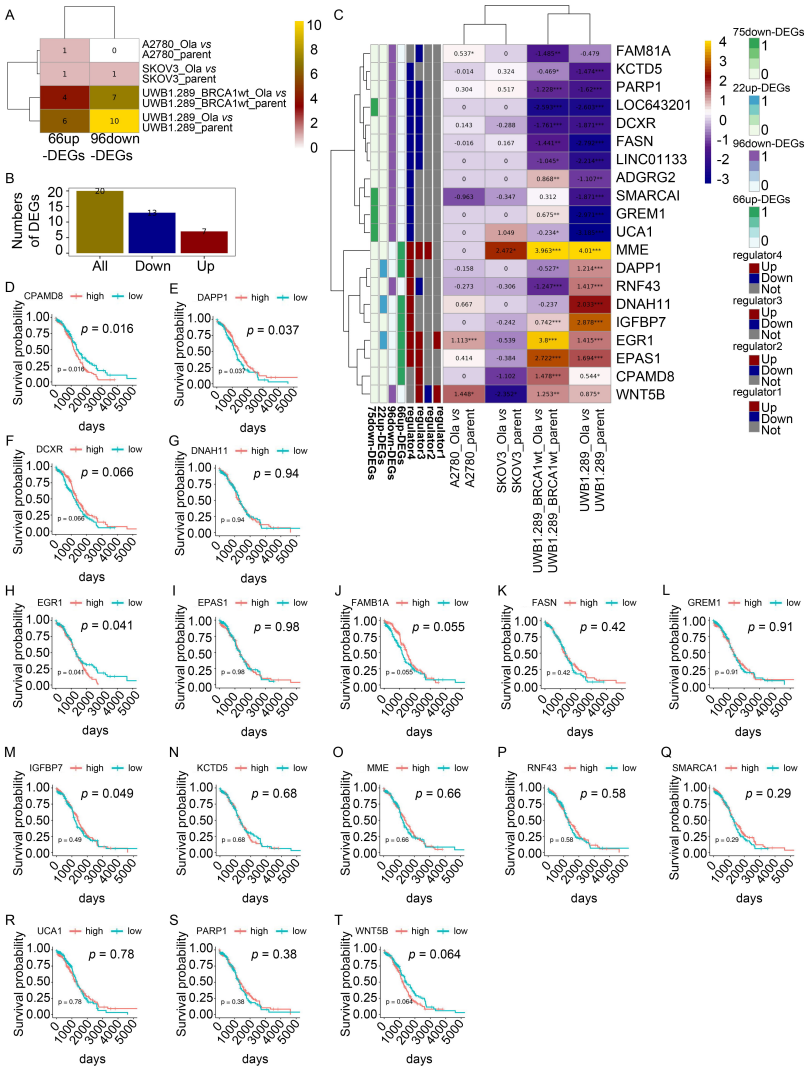

Fig. 7. Differential expression of overlapping significantly differentially expressed genes (DEGs) in ovarian cancer cell models resistant to poly(ADP-ribose) polymerase inhibitors (PARPis) and their prognostic implications. (A,B) Overlap of 66 upregulated DEGs (66up-DEGs) and 96 downregulated DEGs (96down-DEGs) with DEGs from A2780_Ola_resistant, SKOV3_Ola, UWB1.289_BRCA1wt_Ola_resistant, and UWB1.289_Ola_resistant cell groups (A) and the statistics of the number of overlapping genes (B). (C) Differential expression fold change (FC) of 20 overlapping DEGs in A2780_Ola_resistant, SKOV3_Ola, UWB1.289_BRCA1wt_Ola_resistant, and UWB1.289_Ola_resistant groups. (D–T) Kaplan-Meier survival curves based on overall survival (OS) for the following DEGs: *CPAMD8* (D), *DAPP1* (E), *DCXR* (F), *DNAH11* (G), *EGR1* (H), *EPAS1* (I), *FAM81A* (J), *FASN* (K), *GREM1* (L), *IGFBP7* (M), *KCTD5* (N), *MME* (O), *RNF43* (P), *SMARCA1* (Q), *UCA1* (R), *PARP1* (S), *WNT5B* (T). Regulator1, differential expression regulation of genes between A2780_Ola_resistant and A2780_parent groups; regulator2, differential expression regulation of genes between SKOV3_Ola and SKOV3_control groups; regulator3, differential expression regulation of genes between UWB1.289_BRCA1wt_Ola_resistant and UWB1.289_BRCA1wt groups; regulator4, differential expression regulation of genes between UWB1.289_Ola_resistant and UWB1.289 groups; 66up-DEGs, 66 significantly upregulated DEGs consistently expressed in SKOV3 and OVCAR8 cells after 6 months of long-term Olaparib and Niraparib stimulation; 96down-DEGs, 96 significantly downregulated DEGs consistently expressed in SKOV3 and OVCAR8 cells after long-term Olaparib and Niraparib stimulation for 6 months; A2780_Ola_resistant, A2780 cells resistant to Olaparib after long-term treatment (GSE153867 dataset); A2780_parent, The parental A2780 cells from the GSE153867 dataset; UWB1.289_Ola_resistant, UWB1.289 cells resistant to Olaparib after long-term treatment (GSE235980 dataset); UWB1.289, The parental UWB1.289 cells from the GSE235980 dataset without drug treatment; UWB1.289_BRCA1wt, UWB1.289 cells stably overexpressing wild-type BRCA1 without drug treatment (GSE235980 dataset); UWB1.289_BRCA1wt_Ola_resistant, UWB1.289 cells stably overexpressing wild-type BRCA1 and resistant to Olaparib (GSE235980 dataset). *, **, *** represent comparisons with parental cells (A2780_parent, UWB1.289_BRCA1wt_parent, UWB1.289_parent) or cells without drug stimulation (SKOV3_control), respectively, with significance levels of $p < 0.05$, $p < 0.01$, or $p < 0.001$.

ever, within the same clinical stratum (i.e., same grade, stage, or treatment status), differential expression of *EGR1* (high -*vs*- low) did not lead to a significant difference in median OS. Similarly, the expression level of *CPAMD8* (high -*vs*- low) did not significantly impact median OS within any of the analyzed clinical strata (**Supplementary Fig. 6A–D**). Furthermore, analysis of the impact of *CPAMD8* and *EGR1* expression on OS within groups defined by BRCA1/2 mutation status also showed no significant association (**Supplementary Table 4**).

Notably, *EGR1* and *DAPP1* were DEGs that were specifically highly expressed in OVCAR8 cells after 6 months of Olaparib and Niraparib stimulation (Fig. 2M and Fig. 4A,B) and were also significantly elevated in the existing Olaparib-resistant A2780, UWB1.289_BRCA1wt, and/or UWB1.289 cell models (Fig. 7C). *CPAMD8* was predominantly upregulated in SKOV3_Ola_6M, SKOV3_Nira_6M, SKOV3_Nira_3M, and UWB1.289_BRCA1wt_Ola_resistant cells. Functional enrichment analysis revealed that the three genes were primarily enriched in biological processes related to the extracellular matrix (ECM), immune response, and cellular response to stimuli (**Supplementary Fig. 7A–C** and **Supplementary Table 5**), respectively.

Among the three prognostic DEGs, both *CPAMD8* and *EGR1* were significantly upregulated in long-term PARPis stimulation and in PARPis-resistant OC cells (**Supplementary Fig. 4E**). Their upregulation was associated with poorer patient prognosis, suggesting they may serve as key genes in OC resistant to PARPis treatment.

Preliminary Validation of the Effects of CPAMD8 and EGR1 on Ovarian Cancer Sensitivity to Niraparib and Olaparib

The development of mild PARPis resistance in SKOV3 and OVCAR8 cells after 6 months of culture (evidenced by 3.18- to 6.06-fold increases in IC_{50} relative to 2-month cultured parental cells, **Supplementary Figs. 1,2**) prompted the identification of *CPAMD8* and *EGR*1 as candidate resistance genes. To delineate a specific resistance mechanism from a general adaptive response, correlation analysis with 52 known PARPis-resistance genes was performed. *CPAMD8* and *EGR1* showed significant transcriptional correlations with core HRR genes (*BRCA1*, *TP53BP1*, *RAD51*; **Supplementary Table 6**). Furthermore, *EGR1* was bioinformatically linked to HRR and fork stability via potential interactions with *KLF5*, *HLTF*, *BRCA1*, and *EZH2* (**Supplementary Fig. 8**). In addition, we conducted preliminary validation of *CPAMD8* and *EGR1* in PARPis mildly resistant ovarian cancer cells through cellular experiments.

Based on the aforementioned transcriptome sequencing analysis results, the significant upregulation of *CPAMD8* in SKOV3_Nira_6M and SKOV3_Ola_6M cells was further validated through cellular experiments ($p < 0.0001$, Fig. 8A,B). Correspondingly, these cell lines exhibited significantly enhanced cell viability (SKOV3_Nira_6M, $p < 0.0001$; SKOV3_Ola_6M, $p < 0.0001$; Fig. 8C,D) and increased proliferative capacity (Fig. 8E) upon treatment with the respective PARPis. Similarly, *EGR1* expression was significantly elevated in OVCAR8 cells after long-term culture with Niraparib (OVCAR8_Nira_6M) or Olaparib (OVCAR8_Ola_6M) ($p < 0.01$, Fig. 8F,G). These OVCAR8_Nira_6M ($p < 0.0001$, Fig. 8H) and OVCAR8_Ola_6M ($p < 0.0001$, Fig. 8I) cell sublines also demonstrated markedly higher cell viability and enhanced proliferation (Fig. 8J) following PARPis treatment compared with parental controls.

To functionally characterize *CPAMD8*, we performed gain and loss-of-function experiments in the resistant SKOV3 models. siRNA-mediated knockdown of *CPAMD8* ($p < 0.0001$, Fig. 9A–C) significantly sensitized both SKOV3_Nira_6M and SKOV3_Ola_6M cells to PARPis. The combination of *CPAMD8* silencing with Niraparib or Olaparib treatment resulted in a substantial reduction in both proliferative capacity (Fig. 9D) and cell viability ($p < 0.0001$, Fig. 9E,F) compared with PARPis treatment alone. Conversely, overexpression of *CPAMD8* ($p < 0.0001$, Fig. 9A–C) further enhanced the resistant phenotype. The combination of *CPAMD8* overexpression with PARPis treatment led to increased proliferative capacity (Fig. 9D) and cell viability ($p < 0.0001$, Fig. 9E,F) compared with the effects of PARPis alone.

A parallel set of experiments was conducted to assess the role of *EGR1* in the resistant OVCAR8 models. siRNA-mediated knockdown of *EGR1* ($p < 0.05$, Fig. 10A–C) in OVCAR8_Nira_6M and OVCAR8_Ola_6M cells, followed by Niraparib or Olaparib treatment, significantly decreased cell proliferation (Fig. 10D) and viability ($p < 0.001$, Fig. 10E,F) compared with control groups. In contrast, overexpression of *EGR1* ($p < 0.05$, Fig. 10A–C) in these cells significantly increased cell proliferation (Fig. 10D) and viability ($p < 0.0001$, Fig. 10E,F) upon PARPis challenge. These functional outcomes for *EGR1* were analogous to those observed for *CPAMD8*, suggesting a similar potential role in mediating PARPis response.

Discussion

By analyzing the transcriptome of OC cells after 6 months of PARPis treatment and validating these findings using external drug-resistant cell models, *CPAMD8* and *EGR1* were identified as potential targets associated with PARPis resistance. *CPAMD8* (C3 and PZP-like alpha-2-macroglobulin domain-containing 8) is a member of the α-2-macroglobulin family and is involved in immune responses. STRING database analysis revealed that *CPAMD8* interacts with membrane surface collagen (**Supplementary Fig. 7A** and **Supplementary Table 5**). Abnormal expression or function of *CPAMD8* can lead to alterations in the

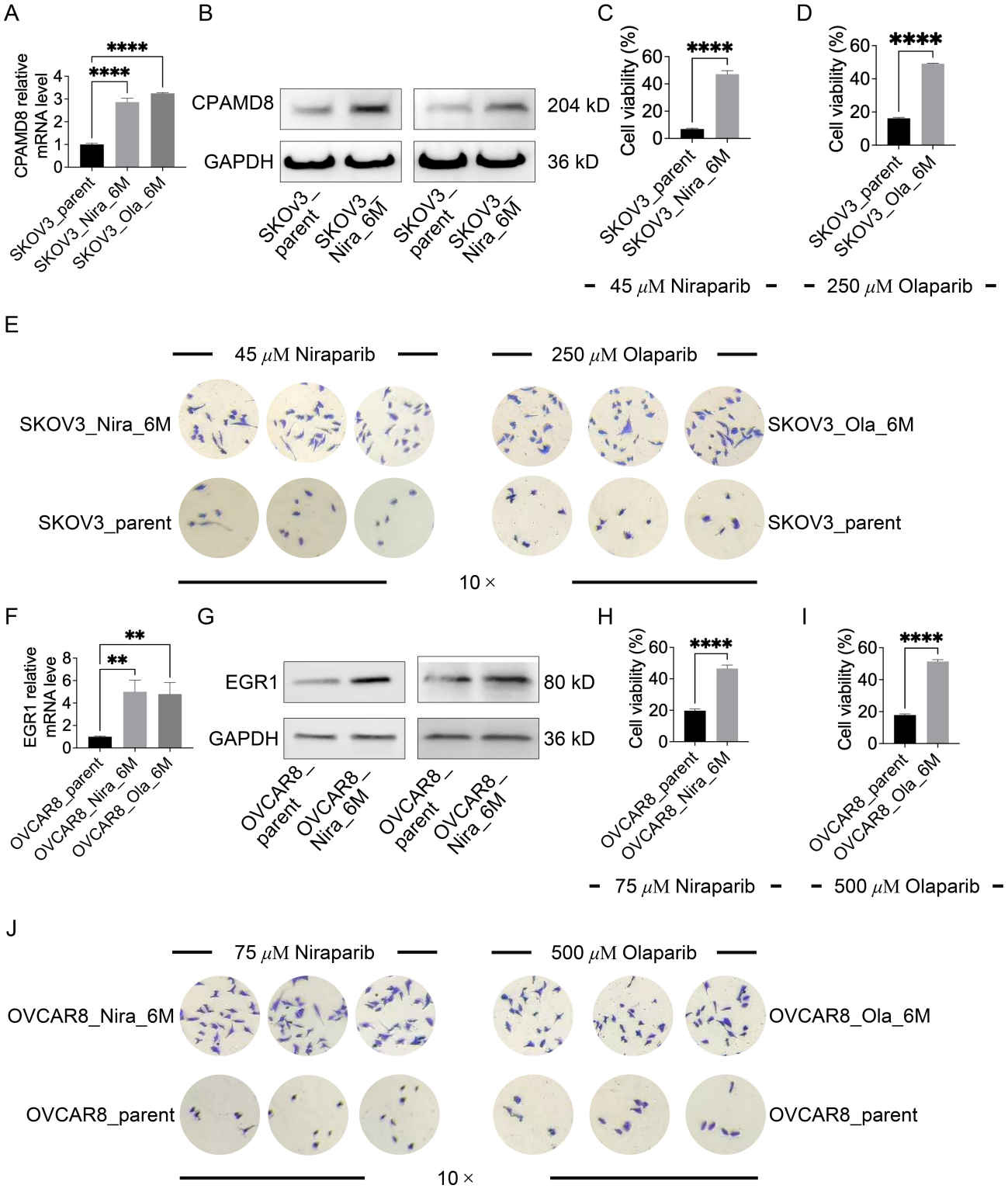

Fig. 8. Elevated expression of *CPAMD8* and *EGR1* in ovarian cancer cells following long-term culture with Niraparib and Olaparib. (A,B) mRNA (A) and protein (B) levels of *CPAMD8* in SKOV3 cells after 6 months of culture with Niraparib (SKOV3_Nira_6M) or Olaparib (SKOV3_Ola_6M). (C–E) Viability (C,D) and proliferative capacity (E, crystal violet staining) of SKOV3_Nira_6M (C) and SKOV3_Ola_6M (D) cells treated with 45 μM Niraparib or 250 μM Olaparib, respectively. (F,G) mRNA (F) and protein (G) levels of *EGR1* in OVCAR8 cells after 6 months of culture with Niraparib (OVCAR8_Nira_6M) or Olaparib (OVCAR8_Ola_6M). (H–J) Viability (H,I) and proliferative capacity (J) crystal violet staining of OVCAR8_Nira_6M (H) and OVCAR8_Ola_6M (I) cells treated with 75 μM Niraparib or 500 μM Olaparib, respectively. **, **** indicate $p < 0.01$ and $p < 0.0001$ versus parental cells, respectively.

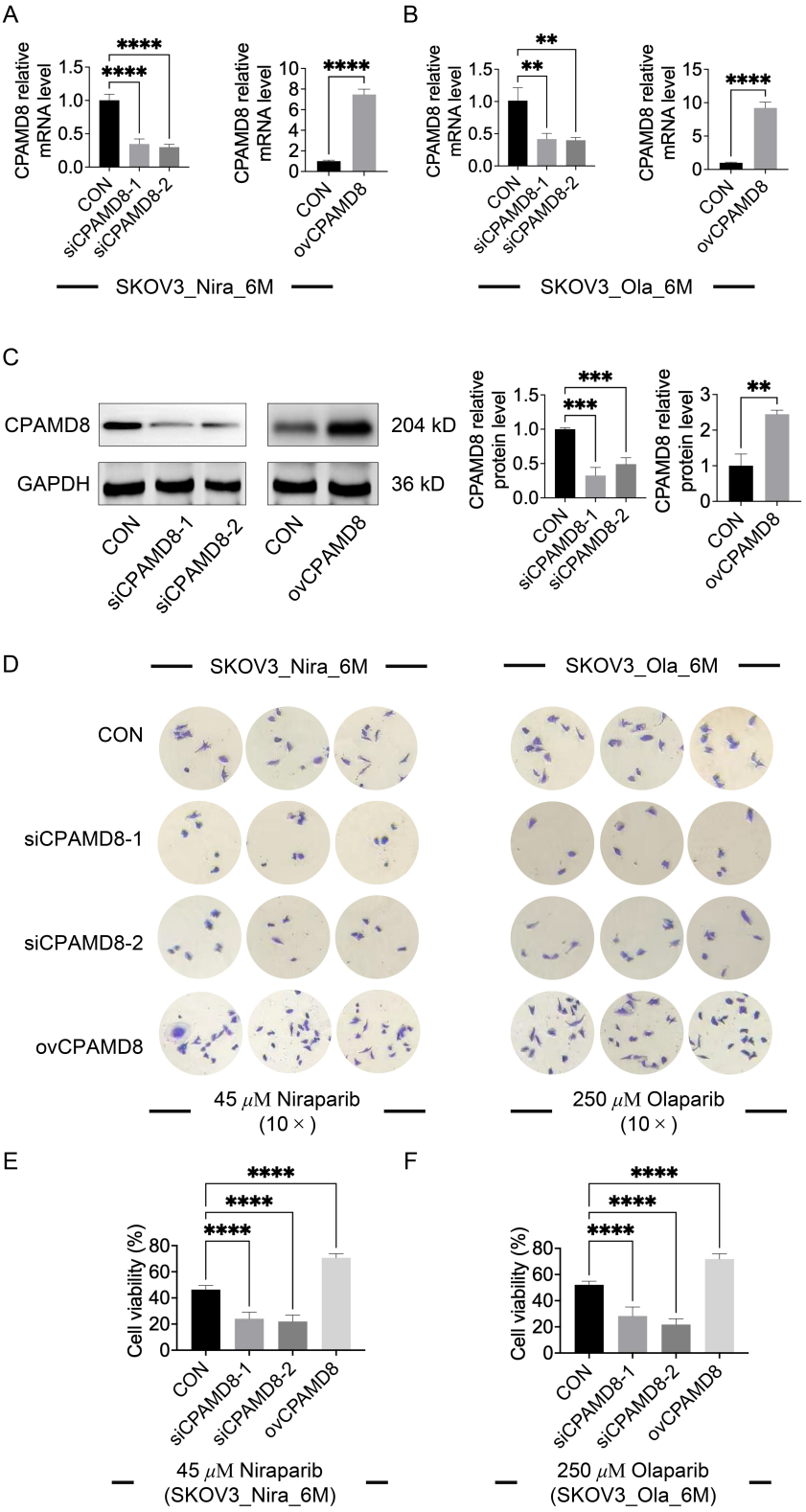

Fig. 9. Effect of *CPAMD8* intervention on the sensitivity of ovarian cancer cells following long-term culture with Niraparib or Olaparib. (A,B) mRNA expression levels of *CPAMD8* in SKOV3_Nira_6M cells (A) and SKOV3_Ola_6M cells (B) after treatment with siRNAs or an overexpression vector. (C) Protein expression levels of *CPAMD8* in SKOV3_Nira_6M cells after treatment with siRNAs or an overexpression vector. (D) Cell proliferative capacity assessed by crystal violet staining following treatment with Niraparib or Olaparib, either alone or in combination with *CPAMD8* siRNA or overexpression vector. (E,F) Viability of SKOV3_Nira_6M cells (E) and SKOV3_Ola_6M cells (F) after treatment with Niraparib (E) or Olaparib (F), either alone or in combination with *CPAMD8* siRNAs or overexpression vector. ** $p < 0.01$, *** $p < 0.001$, **** $p < 0.0001$.

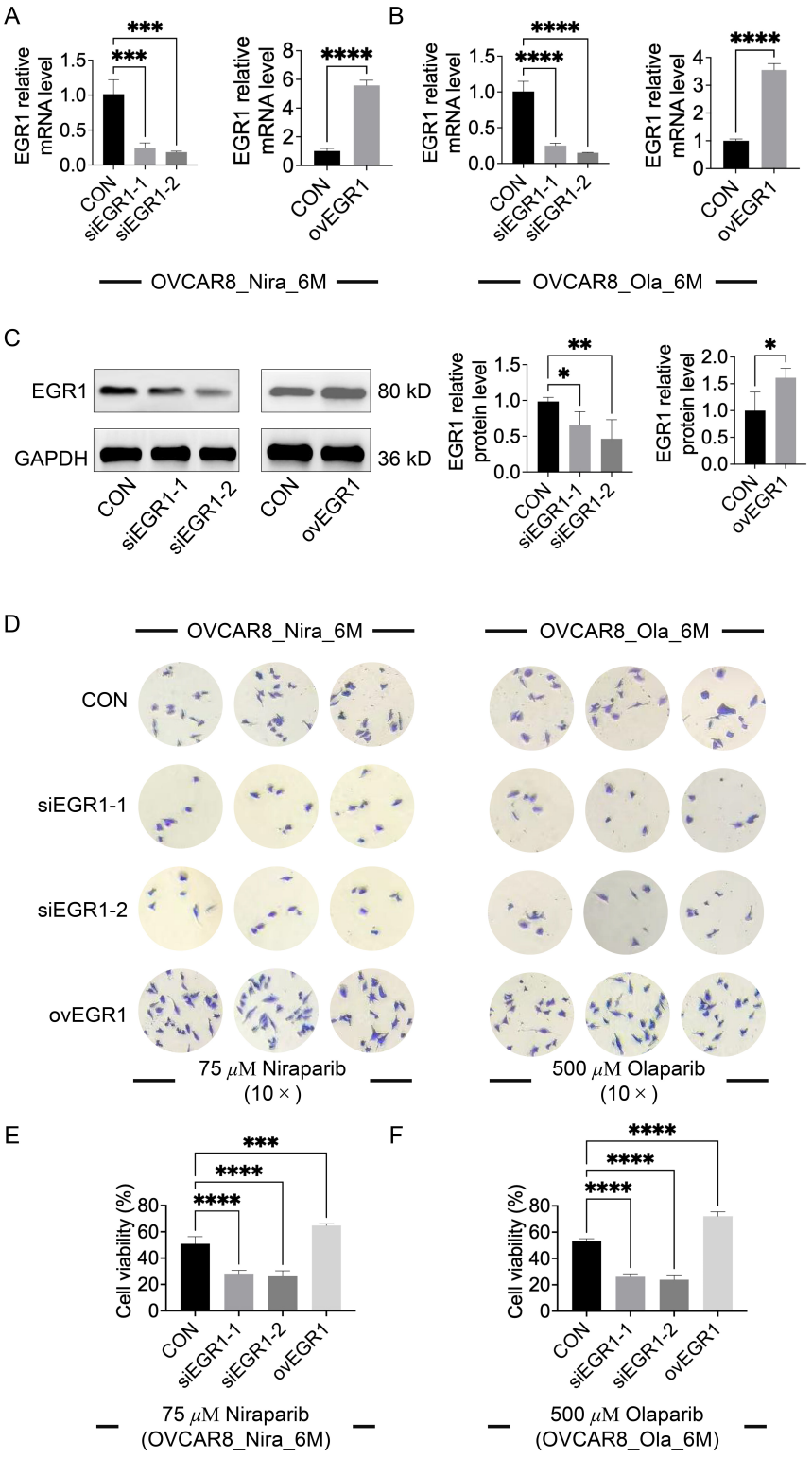

Fig. 10. *EGR1* modulation alters poly(ADP-ribose) polymerase inhibitors sensitivity in ovarian cancer cells following long-term culture with Niraparib or Olaparib. (A,B) *EGR1* mRNA levels in OVCAR8 cells treated with Niraparib (OVCAR8_Nira_6M, A) or Olaparib (SKOV3_Ola_6M, B) for 6 months, following transfection with *EGR1*-targeting siRNA or an overexpression vector. (C) Western blot analysis of *EGR1* protein expression in OVCAR8_Nira_6M cells after siRNA-mediated knockdown or overexpression. (D) Representative images of crystal violet staining showing proliferative capacity of the indicated cell lines after treatment with Niraparib or Olaparib, alone or in combination with *EGR1* modulation. (E,F) Barplot of cell viability in OVCAR8_Nira_6M (E) and SKOV3_Ola_6M (F) cells treated with the corresponding Niraparib or Olaparib, alone or in combination with *EGR1* siRNA or overexpression vector. * $p < 0.05$, ** $p < 0.001$, *** $p < 0.001$, **** $p < 0.0001$.

ECM and defects in cell development, which have been observed in eye diseases such as glaucoma and retinopathy [16,17]. Dysregulation of the ECM is frequently implicated in the development of PARPis-resistant tumors, leading to alterations in cancer cells' responses to mechanical stress, signal transduction, and structural changes, which in turn promote tumor progression, metastasis, and drug resistance [18–21]. The ECM has therefore emerged as an important target in cancer treatment [22]. This suggests that *CPAMD8* regulation of the ECM may play a role in OC resistance to PARPis. While no studies have directly linked *CPAMD8* to tumor resistance, Cervena K's research suggested that *CPAMD8* mutations are associated with the therapeutic response of colon cancer to 5-fluorouracil [23], and Liu SL *et al*. [24] identified *CPAMD8* as a risk factor for nasopharyngeal carcinoma metastasis through transcriptomic analysis. However, research regarding the role of *CPAMD8* in OC resistance to PARPis remains limited.

Early Growth Response 1 (*EGR1*) is a transcriptional regulator that controls cell survival, proliferation, and apoptosis by modulating pathways such as *PI3K-AKT*, hepatocyte growth factor signaling, and responses to DNA damage and ischemia [25]. In pancreatic cancer, *EGR1* regulates MRD1 transcription to induce gemcitabine resistance [26]; it modulates cell cycle D1 expression to promote tamoxifen resistance in breast cancer [27]; and it reprograms oxidative phosphorylation metabolism in B-cell lymphoma to mediate resistance to ibrutinib [28]. These studies indicate that *EGR1* expression is associated with responses to molecular targeted therapies in a variety of cancers. Although *EGR1* has not been linked to PARPis resistance in OC, studies have shown that *EGR1* is upregulated in cells treated with DNA-damaging agents, where it regulates DNA repair mechanisms [29]. The recovery of HR or enhancement of non-homologous end joining (NHEJ) repair after DNA damage is a known mechanism of OC cell resistance to PARPis [30]. This suggests that *EGR1* may promote DNA repair, thereby contributing to the reduced sensitivity of OC to PARPis. While this study only identifies the upregulation of *CPAMD8* and *EGR1* in OC cells after long-term PARPis treatment at the transcriptional level, further experimental work is needed to clarify their specific roles and mechanisms in mediating PARPis resistance in OC.

In addition, we observed distinct expression patterns of *CPAMD8* and *EGR1* across different cell lines. *CPAMD8* was significantly upregulated mainly in SKOV3 cells (**Supplementary Fig. 4E**), which exhibited mild resistance to Niraparib and Olaparib. In contrast, *EGR1* was abnormally expressed in OVCAR8 cells after long-term stimulation with both PARPis (**Supplementary Fig. 4E**). Dimensionality reduction and cluster analysis of overall transcriptional features revealed significant differences between these two cell models, indicating that different OC cell models exhibit varying transcriptomic responses to PARPis. This could be attributed to the fact that SKOV3 and OVCAR8 cells originate from distinct sources and have different genetic backgrounds. SKOV3 cells are derived from ascites of a platinum-sensitive OC patient and display a higher degree of malignancy, whereas OVCAR8 cells originate from a platinum-resistant OC tumor. Therefore, these two cell lines likely reflect the responsiveness of different types of clinical OC patients to PARPis treatment. It is hypothesized that *CPAMD8* is associated with PARPis resistance in platinum-sensitive OC, while *EGR1* is more relevant to PARPis resistance in platinum-resistant OC. Moreover, SKOV3 cells harbor wild-type *TP53*, mutations in *PIK3CA* and *ARID1A*, and amplification of *ERBB2*, while OVCAR8 cells predominantly express mutated *TP53* [31]. This genetic divergence may also contribute to the distinct genomic responses of SKOV3 and OVCAR8 to Olaparib and Niraparib treatment.

Among the DEGs in OC cells treated with PARPis for varying durations, we found that most changes occurred during the mid-phase of treatment (2 and 3 months), and these alterations persisted through the long-term phase (6 months). Notably, *FASN* and *KRT17* were significantly altered in the SKOV3 model, while *ABCB1*, *KRT17*, *MME*, and *CDH2* were significantly altered in the OVCAR8 model. These genes were enriched in biological pathways such as epithelial cell development and differentiation (Fig. 5B). The significant dysregulation of epithelial differentiation pathway genes observed in diverse therapy-resistant malignancies, including PARPis-resistant OC [32–34], drives the loss of epithelial phenotypes and subsequent induction of epithelial-mesenchymal transition (EMT) [35,36]. Molecular profiling confirms this transition through coordinated downregulation of epithelial markers (e.g., *CDH1*, *TJP1*) and upregulation of mesenchymal markers (e.g., *VIM*, *FN1*, *CDH2*, *FSP1*) [37]. Targeting EMT has emerged as a pivotal strategy to suppress tumor progression and re-sensitize cancer cells to therapeutics [38–41], underscoring its mechanistic role in PARPis resistance. Supporting this, Han Y *et al*. [42] demonstrated direct PARPis-induced EMT activation, while Roberts CM *et al*. [43] established that EMT inhibition modulates homologous recombination repair (HRR) gene expression to restore PARPis sensitivity in OC models. The synergistic suppression of EMT through Olaparib-DNA damage response (DDR) inhibitor combinations, accompanied by enhanced cytotoxicity [44], further validates the centrality of EMT in PARPis resistance.

Our longitudinal studies identified EMT-related gene dysregulation in PARPis-adapted OC cell lines. Upregulation of *ABCB1* (multidrug resistance regulator) [45], and *MME* (metastasis promoter) [46] suggests their involvement in PARPis-triggered EMT. Paradoxically, *KRT17* exhibited significant downregulation in SKOV3 cells after 6-month PARPis exposure. Contrasting reports exist regarding the role of *KRT17*: some studies link its loss to E-cadherin deficiency and EMT maintenance [47], while

others identify it as an EMT promoter facilitating invasion [48], necessitating further mechanistic clarification. Similarly unexpected was the downregulation of mesenchymal marker *CDH2* in mildly PARPis-resistant SKOV3 cells. However, a evidence indicates an upregulation of *CDH2* in chemotherapy-resistant tumors [49]. These paradoxical observations highlight context-dependent gene functions in EMT dynamics. For example, *FASN* (fatty acid synthase) provides energy to support rapid cancer cell proliferation [50] and drives tumor metastasis. *KRT17* is upregulated in various malignancies and regulates cytoskeletal composition, influencing cell growth and metastasis [51]. *ABCB1* is involved in the efflux of xenobiotics and mediates multidrug resistance in tumors [52]. *MME* (also known as *CD10*) is implicated in the regulation of the tumor microenvironment, alongside *CDH2* [53], which also contribute to drug resistance in the tumor microenvironment. In summary, while drug resistance was not yet evident at the cellular level during the early stages of drug treatment, changes in certain genes during the middle phase of treatment (2–3 months) suggest an adaptive response that may help cancer cells resist PARPis stimulation in the long term.

Among the prognostic targets identified, *EGR1* demonstrates compelling EMT-regulatory potential. It induces EMT *via* the *P300/SNAI2* axis in pancreatic cancer [54], sustains EMT and angiogenesis in cisplatin-resistant gastric cancer and correlates with proliferative capacity in OC [55,56], suggesting its probable involvement in PARPis-induced EMT. Conversely, no direct evidence links *CPAMD8* to EMT, though its interaction with ECM components—a known EMT modulator—implies potential indirect roles [57]. Our transcriptomic screening nominated *CPAMD8* and *EGR1* as key signature genes in PARPis-adapted OC, yet their EMT-regulatory functions require experimental validation.

This study provided preliminary cellular-level validation of the functional roles of *CPAMD8* and *EGR1* in ovarian cancer cells subjected to long-term culture with PARPis. However, a key limitation lies in the insufficient exploration of the mechanistic underpinnings behind the divergent transcriptional changes observed across different ovarian cancer cell types. Future work will employ well-characterized PARPis-resistant ovarian cancer models to systematically investigate whether the influence of *CPAMD8* and *EGR1* on PARPis sensitivity is consistent across various molecular subtypes of the disease. Furthermore, subsequent studies will specifically validate their functions in EMT-mediated drug resistance and therapy resensitization mechanisms.

Conclusion

By analyzing the transcriptomic changes of OC cell lines at various time points following PARPis treatment, we observed distinct transcriptional alterations between the two cell models, SKOV3 and OVCAR8. Furthermore, *CPAMD8* (upregulated in SKOV3) and *EGR1* (upregulated in OVCAR8), both of which showed consistent upregulation after 6 months of PARPis exposure, were found to be associated with poor prognosis in OC patients. These findings suggest that *CPAMD8* and *EGR1* may play key roles in mediating PARPis resistance and could serve as potential biomarkers for predicting treatment outcomes in OC.

Availability of Data and Materials

RNA sequencing datasets including GSE153867, GSE229119, GSE235980 could obtained from GEO database (https://www.ncbi.nlm.nih.gov/geo/). The datasets used or analyzed during the current study are available from the corresponding author upon reasonable request.

Author Contributions

DZ, SJC and JYL made major contributions to data collection, analysis, and experimental design. TLM and JRL participated in the analysis and visualization of the data. MHZ contributed to the collection and analysis of public databases. TTL contributed to the development of experimental methods used in the study. YZL, YQJ and JLD provided guidance on the research direction, made major contributions to experimental design, and polished the manuscript. All authors contributed to the editing and revision of the original manuscript and approved the final version for publication. All authors have participated sufficiently in the work to take public responsibility for appropriate portions of the content and agreed to be accountable for all aspects of the work in ensuring that questions related to its accuracy or integrity.

Ethics Approval and Consent to Participate

Not applicable.

Acknowledgment

We extend our sincere gratitude to all the personnel who contributed to and supported this research.

Funding

This work was supported by Guangdong Basic and Applied Basic Research Foundation (2023B1515120085, 2024A1515110272 and 2022A1515110197); Huizhou Medical and Health Field Science and Technology Plan Project (2024CZ010270); Shenzhen Science and Technology Innovation Commission (JCYJ20220530152008019); Guangzhou City School (Institute) Joint Funding Project (202201020514 and SL2023A03J00689); the Science and Technology Planning Project of Guangzhou

(2023A03J0264), and the Guangdong Medical Research Foundation (B2023037).

Conflict of Interest

The authors declare no conflict of interest.

Supplementary Material

Supplementary material associated with this article can be found, in the online version, at https://doi.org/10.24976/Discov.Med.202638206.76.

References

[1] Webb PM, Jordan SJ. Global epidemiology of epithelial ovarian cancer. Nature Reviews. Clinical Oncology. 2024; 21: 389–400. https://doi.org/10.1038/s41571-024-00881-3.

[2] Lheureux S, Braunstein M, Oza AM. Epithelial ovarian cancer: Evolution of management in the era of precision medicine. CA: A Cancer Journal for Clinicians. 2019; 69: 280–304. https://doi.org/10.3322/caac.21559.

[3] Xu Q, Li Z. Update on Poly ADP-Ribose Polymerase Inhibitors in Ovarian Cancer With Non-BRCA Mutations. Frontiers in Pharmacology. 2021; 12: 743073. https://doi.org/10.3389/fphar.2021.743073.

[4] González-Martín A, Pothuri B, Vergote I, DePont Christensen R, Graybill W, Mirza MR, *et al*. Niraparib in Patients with Newly Diagnosed Advanced Ovarian Cancer. The New England Journal of Medicine. 2019; 381: 2391–2402. https://doi.org/10.1056/NEJMoa1910962.

[5] Wu XH, Zhu JQ, Yin RT, Yang JX, Liu JH, Wang J, *et al*. Niraparib maintenance therapy in patients with platinum-sensitive recurrent ovarian cancer using an individualized starting dose (NORA): a randomized, double-blind, placebo-controlled phase III trial. Annals of Oncology. 2021; 32: 512–521. https://doi.org/10.1016/j.annonc.2020.12.018.

[6] Pettitt SJ, Lord CJ. Dissecting PARP inhibitor resistance with functional genomics. Current Opinion in Genetics & Development. 2019; 54: 55–63. https://doi.org/10.1016/j.gde.2019.03.001.

[7] Liu M, Zhou X, Sun L, Tan S, Liu T, Xiao W, *et al*. Chronic stress induces platinum and Niraparib resistance in mouse models of ovarian cancer. Experimental Cell Research. 2022; 410: 112935. https://doi.org/10.1016/j.yexcr.2021.112935.

[8] Biegała Ł, Kołat D, Gajek A, Płuciennik E, Marczak A, Śliwińska A, *et al*. Uncovering miRNA-mRNA Regulatory Networks Related to Olaparib Resistance and Resensitization of *BRCA2*^{MUT} Ovarian Cancer PEO1-OR Cells with the ATR/CHK1 Pathway Inhibitors. Cells. 2024; 13: 867. https://doi.org/10.3390/cells13100867.

[9] Li H, Liu ZY, Wu N, Chen YC, Cheng Q, Wang J. PARP inhibitor resistance: the underlying mechanisms and clinical implications. Molecular Cancer. 2020; 19: 107. https://doi.org/10.1186/s12943-020-01227-0.

[10] Waks AG, Cohen O, Kochupurakkal B, Kim D, Dunn CE, Buendia Buendia J, *et al*. Reversion and non-reversion mechanisms of resistance to PARP inhibitor or platinum chemotherapy in BRCA1/2-mutant metastatic breast cancer. Annals of Oncology. 2020; 31: 590–598. https://doi.org/10.1016/j.annonc.2020.02.008.

[11] Tan J, Zheng X, Li M, Ye F, Song C, Xu C, *et al*. C/EBPβ promotes poly(ADP-ribose) polymerase inhibitor resistance by enhancing homologous recombination repair in high-grade serous ovarian cancer. Oncogene. 2021; 40: 3845–3858. https://doi.org/10.1038/s41388-021-01788-4.

[12] Zhang X, Yao J, Li X, Niu N, Liu Y, Hajek RA, *et al*. Targeting polyploid giant cancer cells potentiates a therapeutic response and overcomes resistance to PARP inhibitors in ovarian cancer. Science Advances. 2023; 9: eadf7195. https://doi.org/10.1126/sciadv.adf7195.

[13] Alkema NG, Wisman GBA, van der Zee AGJ, van Vugt MATM, de Jong S. Studying platinum sensitivity and resistance in high-grade serous ovarian cancer: Different models for different questions. Drug Resistance Updates. 2016; 24: 55–69. https://doi.org/10.1016/j.drup.2015.11.005.

[14] Feng T, Wei D, Zhao J, Li Q, Guo P, Yang X, *et al*. Construction of enzalutamide-resistant cell model of prostate cancer and preliminary screening of potential drug-resistant genes. Experimental Biology and Medicine. 2021; 246: 1776–1787. https://doi.org/10.1177/15353702211012625.

[15] Qin X, Liu J, Chen X, Zhong FF, Yang Y, Zeng Y, *et al*. Establishment of Cytarabine-resistant Acute Lymphoblastic Leukemia Cell Lines and Its Resistance Mechanism. Zhongguo Shi Yan Xue Ye Xue Za Zhi. 2021; 29: 1403–1410. https://doi.org/10.19746/j.cnki.issn.1009-2137.2021.05.006. (In Chinese)

[16] Bonet-Fernández JM, Aroca-Aguilar JD, Corton M, Ramírez AI, Alexandre-Moreno S, García-Antón MT, *et al*. CPAMD8 loss-of-function underlies non-dominant congenital glaucoma with variable anterior segment dysgenesis and abnormal extracellular matrix. Human Genetics. 2020; 139: 1209–1231. https://doi.org/10.1007/s00439-020-02164-0.

[17] Siggs OM, Souzeau E, Taranath DA, Dubowsky A, Chappell A, Zhou T, *et al*. Biallelic CPAMD8 Variants Are a Frequent Cause of Childhood and Juvenile Open-Angle Glaucoma. Ophthalmology. 2020; 127: 758–766. https://doi.org/10.1016/j.ophtha.2019.12.024.

[18] Roy AM, Iyer R, Chakraborty S. The extracellular matrix in hepatocellular carcinoma: Mechanisms and therapeutic vulnerability. Cell Reports. Medicine. 2023; 4: 101170. https://doi.org/10.1016/j.xcrm.2023.101170.

[19] Gonzalez-Molina J, Moyano-Galceran L, Single A, Gultekin O, Alsalhi S, Lehti K. Chemotherapy as a regulator of extracellular matrix-cell communication: Implications in therapy resistance. Seminars in Cancer Biology. 2022; 86: 224–236. https://doi.org/10.1016/j.semcancer.2022.03.012.

[20] Valmiki S, Aid MA, Chaitou AR, Zahid M, Valmiki M, Fawzy P, *et al*. Extracellular Matrix: A Treasure Trove in Ovarian Cancer Dissemination and Chemotherapeutic Resistance. Cureus. 2021; 13: e13864. https://doi.org/10.7759/cureus.13864.

[21] Brown Y, Hua S, Tanwar PS. Extracellular matrix in high-grade serous ovarian cancer: Advances in understanding of carcinogenesis and cancer biology. Matrix Biology. 2023; 118: 16–46. https://doi.org/10.1016/j.matbio.2023.02.004.

[22] Jiang Y, Zhang H, Wang J, Liu Y, Luo T, Hua H. Targeting extracellular matrix stiffness and mechanotransducers to improve cancer therapy. Journal of Hematology & Oncology. 2022; 15: 34. https://doi.org/10.1186/s13045-022-01252-0.

[23] Cervena K, Pardini B, Urbanova M, Vodenkova S, Eva P, Veskrnova V, *et al*. Mutational landscape of plasma cell-free DNA identifies molecular features associated with therapeutic response in patients with colon cancer. A pilot study. Mutagenesis. 2021; 36: 358–368. https://doi.org/10.1093/mutage/geab024.

[24] Liu SL, Sun XS, Chen QY, Liu ZX, Bian LJ, Yuan L, *et al*. Development and validation of a transcriptomics-based gene signature to predict distant metastasis and guide induction chemotherapy in locoregionally advanced nasopharyngeal carcinoma. Eu-

ropean Journal of Cancer. 2022; 163: 26–34. https://doi.org/10.1016/j.ejca.2021.12.017.

[25] Wang B, Guo H, Yu H, Chen Y, Xu H, Zhao G. The Role of the Transcription Factor EGR1 in Cancer. Frontiers in Oncology. 2021; 11: 642547. https://doi.org/10.3389/fonc.2021.642547.

[26] Yang Z, Chen F, Wei D, Chen F, Jiang H, Qin S. EGR1 mediates MDR1 transcriptional activity regulating gemcitabine resistance in pancreatic cancer. BMC Cancer. 2024; 24: 268. https://doi.org/10.1186/s12885-024-12005-2.

[27] Marks BA, Pipia IM, Mukai C, Horibata S, Rice EJ, Danko CG, *et al*. GDNF-RET signaling and EGR1 form a positive feedback loop that promotes tamoxifen resistance via cyclin D1. BMC Cancer. 2023; 23: 138. https://doi.org/10.1186/s12885-023-10559-1.

[28] Liu Y, Kimpara S, Hoang NM, Daenthanasanmak A, Li Y, Lu L, *et al*. EGR1-mediated metabolic reprogramming to oxidative phosphorylation contributes to ibrutinib resistance in B-cell lymphoma. Blood. 2023; 142: 1879–1894. https://doi.org/10.1182/blood.2023020142.

[29] Quiñones A, Dobberstein KU, Rainov NG. The egr-1 gene is induced by DNA-damaging agents and non-genotoxic drugs in both normal and neoplastic human cells. Life Sciences. 2003; 72: 2975–2992. https://doi.org/10.1016/s0024-3205(03)00230-3.

[30] Wang L, Wang Q, Xu Y, Cui M, Han L. Advances in the Treatment of Ovarian Cancer Using PARP Inhibitors and the Underlying Mechanism of Resistance. Current Drug Targets. 2020; 21: 167–178. https://doi.org/10.2174/1389450120666190925123507.

[31] Domcke S, Sinha R, Levine DA, Sander C, Schultz N. Evaluating cell lines as tumour models by comparison of genomic profiles. Nature Communications. 2013; 4: 2126. https://doi.org/10.1038/ncomms3126.

[32] Błaszczak E, Miziak P, Odrzywolski A, Baran M, Gumbarewicz E, Stepulak A. Triple-Negative Breast Cancer Progression and Drug Resistance in the Context of Epithelial-Mesenchymal Transition. Cancers. 2025; 17: 228. https://doi.org/10.3390/cancers17020228.

[33] Wang X, Eichhorn PJA, Thiery JP. TGF-β, EMT, and resistance to anti-cancer treatment. Seminars in Cancer Biology. 2023; 97: 1–11. https://doi.org/10.1016/j.semcancer.2023.10.004.

[34] Cheng A, Rao Q, Liu Y, Huang C, Li J, Huo C, *et al*. Genomic and expressional dynamics of ovarian cancer cell lines in PARPi treatment revealed mechanisms of acquired resistance. Gynecologic Oncology. 2022; 167: 502–512. https://doi.org/10.1016/j.ygyno.2022.10.011.

[35] Singh D, Siddique HR. Epithelial-to-mesenchymal transition in cancer progression: unraveling the immunosuppressive module driving therapy resistance. Cancer Metastasis Reviews. 2024; 43: 155–173. https://doi.org/10.1007/s10555-023-10141-y.

[36] Brabletz S, Schuhwerk H, Brabletz T, Stemmler MP. Dynamic EMT: a multi-tool for tumor progression. The EMBO Journal. 2021; 40: e108647. https://doi.org/10.15252/embj.2021108647.

[37] Fontana R, Mestre-Farrera A, Yang J. Update on Epithelial-Mesenchymal Plasticity in Cancer Progression. Annual Review of Pathology. 2024; 19: 133–156. https://doi.org/10.1146/annurev-pathmechdis-051222-122423.

[38] Zhang N, Ng AS, Cai S, Li Q, Yang L, Kerr D. Novel therapeutic strategies: targeting epithelial-mesenchymal transition in colorectal cancer. The Lancet. Oncology. 2021; 22: e358–e368. https://doi.org/10.1016/S1470-2045(21)00343-0.

[39] Huang Y, Hong W, Wei X. The molecular mechanisms and therapeutic strategies of EMT in tumor progression and metastasis. Journal of Hematology & Oncology. 2022; 15: 129. https://doi.org/10.1186/s13045-022-01347-8.

[40] Ren Y, Mao X, Xu H, Dang Q, Weng S, Zhang Y, *et al*. Ferroptosis and EMT: key targets for combating cancer progression and therapy resistance. Cellular and Molecular Life Sciences. 2023; 80: 263. https://doi.org/10.1007/s00018-023-04907-4.

[41] Zhang H, Steed A, Co M, Chen X. Cancer stem cells, epithelial-mesenchymal transition, ATP and their roles in drug resistance in cancer. Cancer Drug Resistance. 2021; 4: 684–709. https://doi.org/10.20517/cdr.2021.32.

[42] Han Y, Li CW, Hsu JM, Hsu JL, Chan LC, Tan X, *et al*. Metformin reverses PARP inhibitors-induced epithelial-mesenchymal transition and PD-L1 upregulation in triple-negative breast cancer. American Journal of Cancer Research. 2019; 9: 800–815.

[43] Roberts CM, Rojas-Alexandre M, Hanna RE, Lin ZP, Ratner ES. Transforming Growth Factor Beta and Epithelial to Mesenchymal Transition Alter Homologous Recombination Repair Gene Expression and Sensitize BRCA Wild-Type Ovarian Cancer Cells to Olaparib. Cancers. 2023; 15: 3919. https://doi.org/10.3390/cancers15153919.

[44] Gralewska P, Biegała Ł, Gajek A, Szymczak-Pajor I, Marczak A, Śliwińska A, *et al*. Olaparib Combined with DDR Inhibitors Effectively Prevents EMT and Affects miRNA Regulation in *TP53*-Mutated Epithelial Ovarian Cancer Cell Lines. International Journal of Molecular Sciences. 2025; 26: 693. https://doi.org/10.3390/ijms26020693.

[45] da Costa KM, Freire-de-Lima L, da Fonseca LM, Previato JO, Mendonça-Previato L, Valente RDC. ABCB1 and ABCC1 Function during TGF-β-Induced Epithelial-Mesenchymal Transition: Relationship between Multidrug Resistance and Tumor Progression. International Journal of Molecular Sciences. 2023; 24: 6046. https://doi.org/10.3390/ijms24076046.

[46] You Y, Tian Z, Du Z, Wu K, Xu G, Dai M, *et al*. M1-like tumor-associated macrophages cascade a mesenchymal/stem-like phenotype of oral squamous cell carcinoma via the IL6/Stat3/THBS1 feedback loop. Journal of Experimental & Clinical Cancer Research. 2022; 41: 10. https://doi.org/10.1186/s13046-021-02222-z.

[47] Li M, Rao X, Cui Y, Zhang L, Li X, Wang B, *et al*. The keratin 17/YAP/IL6 axis contributes to E-cadherin loss and aggressiveness of diffuse gastric cancer. Oncogene. 2022; 41: 770–781. https://doi.org/10.1038/s41388-021-02119-3.

[48] Meng F, Dai L. Transcription factors TP63 facilitates malignant progression of thyroid cancer by upregulating KRT17 expression and inducing epithelial-mesenchymal transition. Growth Factors. 2023; 41: 71–81. https://doi.org/10.1080/08977194.2023.2184656.

[49] Xu JY, Tian MQ, Yang R, Li ZX, Lin ZH, Wang YF, *et al*. Integrated Analyses Identify CDH2 as a Hub Gene Associated with Cisplatin Resistance and Prognosis in Ovarian Cancer. International Journal of Molecular Sciences. 2026; 27: 713. https://doi.org/10.3390/ijms27020713.

[50] Vanauberg D, Schulz C, Lefebvre T. Involvement of the pro-oncogenic enzyme fatty acid synthase in the hallmarks of cancer: a promising target in anti-cancer therapies. Oncogenesis. 2023; 12: 16. https://doi.org/10.1038/s41389-023-00460-8.

[51] Zhang H, Zhang Y, Xia T, Lu L, Luo M, Chen Y, *et al*. The Role of Keratin17 in Human Tumours. Frontiers in Cell and Developmental Biology. 2022; 10: 818416. https://doi.org/10.3389/fcell.2022.818416.

[52] Skinner KT, Palkar AM, Hong AL. Genetics of *ABCB1* in Cancer. Cancers. 2023; 15: 4236. https://doi.org/10.3390/cancers15174236.

[53] Parker J, Hockney S, Blaschuk OW, Pal D. Targeting N-cadherin (CDH2) and the malignant bone marrow microenvironment in acute leukaemia. Expert Reviews in Molecular Medicine. 2023; 25: e16. https://doi.org/10.1017/erm.2023.13.

[54] Wang Y, Qin C, Zhao B, Li Z, Li T, Yang X, *et al*. EGR1 induces

EMT in pancreatic cancer via a P300/SNAI2 pathway. Journal of Translational Medicine. 2023; 21: 201. https://doi.org/10.1186/s12967-023-04043-4.

[55] Geng T, Sun Q, He J, Chen Y, Cheng W, Shen J, *et al*. CXXC5 drove inflammation and ovarian cancer proliferation via transcriptional activation of ZNF143 and EGR1. Cellular Signalling. 2024; 119: 111180. https://doi.org/10.1016/j.cellsig.2024.111180.

[56] Ren Y, Xu R, Zhang D, Su L, Jin Y, Li N, *et al*. NFIC suppressed the epithelial ovarian cancer via modulating the balance of PTEN/TGFβ1/EGR1/BRD4 and SP1/EZH2 induced Inhibition of TBX2/MMPs signaling. Scientific Reports. 2025; 15: 26593. https://doi.org/10.1038/s41598-025-09653-0.

[57] Scott LE, Weinberg SH, Lemmon CA. Mechanochemical Signaling of the Extracellular Matrix in Epithelial-Mesenchymal Transition. Frontiers in Cell and Developmental Biology. 2019; 7: 135. https://doi.org/10.3389/fcell.2019.00135.